High-Throughput Reclassification of *SCN5A* Variants

Andrew M. Glazer,[1] Yuko Wada,[1] Bian Li,[2] Ayesha Muhammad,[1] Olivia R. Kalash,[1] Matthew J. O'Neill,[1] Tiffany Shields,[1] Lynn Hall,[1] Laura Short,[1] Marcia A. Blair,[1] Brett M. Kroncke,[1,3] John A. Capra,[2] and Dan M. Roden[1,3,4,*]

Partial or complete loss-of-function variants in *SCN5A* are the most common genetic cause of the arrhythmia disorder Brugada syndrome (BrS1). However, the pathogenicity of *SCN5A* variants is often unknown or disputed; 80% of the 1,390 *SCN5A* missense variants observed in at least one individual to date are variants of uncertain significance (VUSs). The designation of VUS is a barrier to the use of sequence data in clinical care. We selected 83 variants: 10 previously studied control variants, 10 suspected benign variants, and 63 suspected Brugada syndrome-associated variants, selected on the basis of their frequency in the general population and in individuals with Brugada syndrome. We used high-throughput automated patch clamping to study the function of the 83 variants, with the goal of reclassifying variants with functional data. The ten previously studied controls had functional properties concordant with published manual patch clamp data. All 10 suspected benign variants had wild-type-like function. 22 suspected BrS variants had loss of channel function (<10% normalized peak current) and 22 variants had partial loss of function (10%–50% normalized peak current). The previously unstudied variants were initially classified as likely benign (n = 2), likely pathogenic (n = 10), or VUSs (n = 61). After the patch clamp studies, 16 variants were benign/likely benign, 45 were pathogenic/likely pathogenic, and only 12 were still VUSs. Structural modeling identified likely mechanisms for loss of function including altered thermostability and disruptions to alpha helices, disulfide bonds, or the permeation pore. High-throughput patch clamping enabled reclassification of the majority of tested VUSs in *SCN5A*.

Introduction

Variants in the cardiac sodium channel gene *SCN5A* (which encodes the protein $Na_V1.5$) have been linked to many arrhythmia and cardiac conditions, including Brugada syndrome (BrS [MIM: 601144]),[1] long QT syndrome (LQT [MIM: 603830]),[2] dilated cardiomyopathy (MIM: 601154),[3] cardiac conduction disease (MIM: 113900),[4] and sick sinus syndrome (MIM: 608567).[5] BrS is diagnosed by a characteristic ECG pattern (ST-segment elevation in the right precordial leads) at baseline or upon drug challenge and is associated with an increased risk for sudden cardiac death.[6] *SCN5A* loss-of-function variants are the most common (and in fact, the only ClinGen-validated)[7] genetic cause of BrS, and are present in approximately 30% of case subjects (BrS1).[1,8,9] Variants that destabilize fast inactivation of the channel and generate a persistent ("late") current are associated with LQT.[10,11] The risk of sudden cardiac death in individuals with Brugada syndrome can be partially prevented, for example with implantable defibrillators. Therefore, incidentally discovered *SCN5A* variants that are pathogenic or likely pathogenic for BrS are considered actionable and reportable.[12]

A multi-center study of 2,111 unrelated individuals with Brugada syndrome discovered 293 distinct *SCN5A* variants, including 225 variants present in only one individual.[1] This result indicates that Brugada syndrome risk is distributed among many different, rare *SCN5A* variants. A large body of work reporting phenotypes of *SCN5A* variant carriers and studying these variants by *in vitro* patch clamping has established the link between partial or total loss of $Na_V1.5$ function and Brugada syndrome.[1,13–16] In a recent literature curation, we identified 1,712 *SCN5A* variants that have been observed to date in at least one individual in the literature or in the genome aggregation database (gnomAD).[10] The strongest predictor of a variant's association with Brugada syndrome was a partial or total reduction in peak current recorded during voltage clamp experiments in heterologous expression systems (mainly HEK293 cells).[10] Additionally, a weaker association was observed between a variant's Brugada syndrome association and its $V_{1/2}$ activation, the voltage that elicits half-maximal channel activation.

Because *SCN5A* variants linked to Brugada syndrome have incomplete penetrance, assessment of variant risk using phenotypic data in single variant carriers can be minimally informative.[17] Nevertheless, an important challenge is to accurately classify variants, especially when only limited phenotype data are available.[18] The American College of Medical Genetics and Genomics (ACMG) classification scheme uses 28 criteria to classify variants into 5 categories: pathogenic, likely pathogenic, benign, likely benign, or variant of uncertain significance (VUS).[19] Two "strong evidence" ACMG criteria rely on *in vitro* functional data: pathogenic strong criterion 3 (PS3, well-established functional variant studies show a deleterious effect) and

[1]Vanderbilt Center for Arrhythmia Research and Therapeutics, Division of Clinical Pharmacology, Department of Medicine, Vanderbilt University Medical Center, Nashville, TN 37232, USA; [2]Department of Biological Sciences, Center for Structural Biology, and Vanderbilt Genetics Institute, Vanderbilt University, Nashville, TN 37235, USA; [3]Department of Pharmacology, Vanderbilt University Medical Center, Nashville, TN 37232, USA; [4]Department of Biomedical Informatics, Vanderbilt University Medical Center, Nashville, TN 37232, USA
*Correspondence: dan.roden@vumc.org
https://doi.org/10.1016/j.ajhg.2020.05.015.

benign strong criterion 3 (BS3, well-established functional variant studies show no deleterious effect).

Conventionally, variants in ion channels such as *SCN5A* have been assessed by time-intensive manual patch clamping of variants in heterologous expression. Recently, automated high-throughput patch clamp devices have allowed the rapid evaluation of dozens of variants in ion channel genes, including the arrhythmia-associated genes *KCNQ1* and *KCNH2*.[20–22] In this study, we use automated patch clamping to study 83 *SCN5A* variants. We identify 44 new partial or total loss-of-function variants and reclassify 49/61 variants of uncertain significance. We further use structural modeling to identify likely mechanisms of $Na_V1.5$ loss of function, including altered thermostability and disruptions to critical protein features.

Material and Methods

Selection of Variants

83 variants were studied by automated patch clamping (Figure 1): 10 previously studied controls, 10 suspected benign variants, and 63 suspected BrS variants. The previously studied variants were chosen because they had a spectrum of normal and abnormal channel function, representing multiple types of perturbations to the channel. The suspected BrS variants were selected because they appeared in at least one case of BrS in the literature and were relatively rare or absent in the gnomAD database of putative controls (minor allele frequency of 0 to 5e−5, except for p.Asp1243Asn which had 5 BrS cases and an allele frequency of 1.4e−4; Figure 2B, Table S1).[10,23] In contrast, the suspected benign variants were observed in multiple unaffected or gnomAD individuals (minor allele frequency of 5e−5 to 3e−4), but never in cases of BrS or LQT in the literature (Figure 2B, Table S1). p.Arg1958Ter was also classified as a suspected BrS variant because it is a nonsense variant. However, to our knowledge, it has not been observed in any individuals with BrS (Figure 2B, Table S1).

SCN5A Mutagenesis

To facilitate mutagenesis, a "zone" system was developed that divided the 6 kilobase *SCN5A* cDNA into 8 zones of ~750 bp each (Table S2). These zones were separated by restriction enzyme sites already present in the *SCN5A* coding sequence or introduced with synonymous mutations. Mutagenesis primers were designed with the online QuikChange primer design tool. All mutagenesis primers are listed in Table S3. The QuikChange Lighting Multi kit (Agilent) was used to perform the mutagenesis with one primer/mutation, following manufacturer's instructions. Mutants were created in a small (<4 kilobase) plasmid containing the zone of interest. Following sequence verification, mutant zones were moved with the appropriate restriction enzymes into a plasmid containing an AttB recombination site and a full-length *SCN5A*:IRES:mCherry-blasticidinR (Figure S1). This plasmid was modified from a previously published promoterless dsRed-Express-derivative plasmid designed for rapid stable line generation.[24] This modification introduced *SCN5A* into the plasmid and included the generation of a mCherry-blasticidinR fusion protein. For all plasmids, the entire *SCN5A* coding region was Sanger sequenced to confirm that the variant of interest was included and to verify that there were no off-target variants. The "wild-type" *SCN5A* used in this study had the more common His allele of the p.His558Arg polymorphism (rs1805124) and the most common splice isoform in the heart, a 2,015-amino acid sequence (not counting the stop codon) that includes deletion of the Gln1077 residue (ENST00000443581). However, the variants are named according to the 2,016-amino acid Gln1077-included isoform (ENST00000333535), as is standard in the literature.

Stable *SCN5A*-Expressing Cell Lines

Human Embryonic Kidney HEK293T "negative selection" landing pad cells were used, which express Blue Fluorescent Protein and an activatable iCasp caspase from a tetracycline-sensitive promoter.[25] In these cells, an AttP integration site is located in between the promoter and the BFP/iCasp. Bxb1 integrase-mediated integration of a plasmid containing an AttB site at the genomic AttP location disrupts the expression of BFP/iCasp. After integration of an AttB-containing *SCN5A*:IRES:mCherry:blasticidinR plasmid, these cells switch to expression of *SCN5A* and an mCherry-blasticidinR fusion protein. Cells were cultured at 37°C in a humidified 95% air/5% CO_2 incubator in "HEK media": Dulbecco's Eagle's medium supplemented with 10% fetal bovine serum, 1% non-essential amino acids, and 1% penicillin/streptomycin. On day −1, cells were plated in 12-well plates. On day 0, each well was transfected with 2.1 μl FuGENE 6 (Promega), 600 ng of the mutant *SCN5A* plasmid, and 100 ng of a plasmid expressing Bxb1 recombinase (a gift from Pawel Pelczar,[26] Addgene plasmid #51271). On day 1, cells were washed with HEK media to remove the FuGENE reagent. On day 3, the cells were exposed to 1 μg/mL doxycycline (Sigma) in HEK media to induce expression of either the *SCN5A* mutant or iCasp9 in non-integrated cells from the Tet-sensitive promoter. On day 5, cells were exposed to 1 μg/mL doxycycline, 100 μg/mL blasticidin S (Sigma), and 10 nM AP1903 (MedChemExpress) in HEK media. The blasticidin selected for expression of the blasticidin resistance gene present on the *SCN5A* plasmid. The AP1903 activated the iCasp caspase protein expressed from non-integrated cells; this resulted in selection against non-integrated cells. Cells were exposed to doxycycline+blasticidin+AP1903 in HEK media for 4–7 days to select for integrated cells, passaging cells as needed. Less than 48 h prior to the SyncroPatch experiment, cells were analyzed by analytical flow cytometry on a BD Fortessa 4-laser instrument to determine the percentage of cells that were mCherry-positive, Blue Fluorescent Protein-negative, indicating cells with successful integration of the *SCN5A* plasmid. BFP was measured by excitation at 405 and emission at 450/50 and mCherry was measured by excitation at 561 and emission at 610/20.

Automated Patch Clamping

Cells were patch clamped with the SyncroPatch 384PE automated patch clamping device (Nanion). To prepare cells for patch clamping, cells were washed in PBS, treated with Accutase (Millipore-Sigma) for 3 min at 37°C, then recovered in CHO-S-serum free media (GIBCO). Cells were pelleted and resuspended in divalent-free reference solution (DVF) at ~200,000–400,000 cells/mL. DVF contained (mM) NaCl 140, KCl 4, alpha-D(+)-glucose 5, HEPES 10 (pH 7.4) adjusted with NaOH. Cells were then added to a medium resistance (4–6 MΩ) 384-well recording chamber with 1 patch aperture per well (NPC-384, Nanion), which contained DVF and internal solution: CsCl 10, NaCl 10, CsF 110, EGTA 10, HEPES 10 (pH 7.2) adjusted with CsOH. Next, to

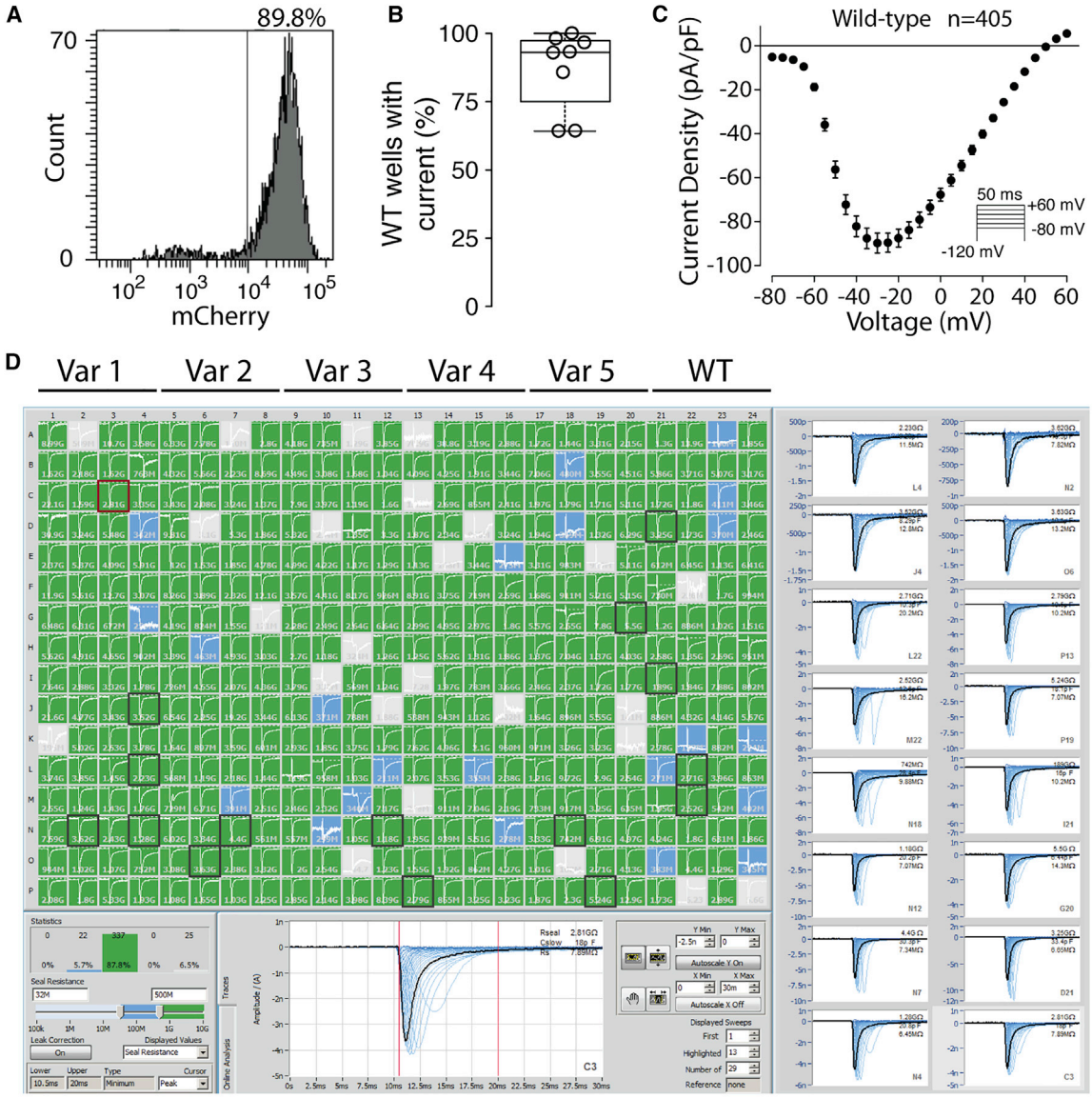

Figure 1. Molecular and Functional Expression of *SCN5A*

(A) Flow cytometry plot of representative wild-type stable cell line. Histogram of mCherry signal is shown. 89.8% of cells expressed a high-level of mCherry, indicating successful plasmid integration.

(B) Boxplot of percentage of wild-type wells with $Na_V1.5$-like current across eight independent transfections. Only wells with a cell passing seal resistance and capacitance criteria (see Material and Methods) were considered.

(C) Wild-type current density-voltage plot, averaged across 405 wild-type cells passing quality control (seal resistance, capacitance, in voltage control, and minimum peak current criteria, see Material and Methods). The predicted reversal potential given the internal and external solutions used in this study is 45.3 mV. Error bars indicate SEM.

(D) Example SyncroPatch experiment. A typical experiment studied 5 variants and wild-type on a single 384-well chip. In this experiment all 5 variants had wild-type-like currents. Green wells indicate a cell with seal resistance >0.5 GΩ, blue wells indicate a cell with seal resistance 0.2–0.5 GΩ (not included in analysis), and gray wells indicate no cell present or a cell with seal resistance <0.2 GΩ (not included in analysis). Randomly selected cells with seals >0.5GΩ are highlighted with a black square and displayed on the right.

enhance seal resistance, 50% of the DVF was exchanged with a calcium-containing seal enhancing solution: NaCl 80, NMDG 60, KCl 4, $MgCl_2$ 1, $CaCl_2$ 10, alpha-D(+)-glucose 5, HEPES 10 (pH 7.4) adjusted with HCl. The cells were washed three times in external recording solution: NaCl 80, NMDG 60, KCl 4, $MgCl_2$ 1, $CaCl_2$ 2, alpha-D(+)-glucose 5, HEPES 10 (pH 7.4) adjusted with HCl. Currents elicited in response to activation, inactivation, and recovery from inactivation protocols were then recorded (Figure S2). A late current measurement was captured every 5 s. After 1 min, 50% of the external solution was exchanged with external solution containing 200 μM tetracaine hydrochloride (Sigma; effective concentration 100 μM tetracaine). After tetracaine addition, late current measurements were obtained every 5 s for 1 additional minute. At least 10 cells expressing wild-type *SCN5A* were included for comparison in each SyncroPatch experiment (Figure 1), and at least 2 independent transfections and at least 10 replicate cells were studied per mutant. Recordings were performed at room temperature.

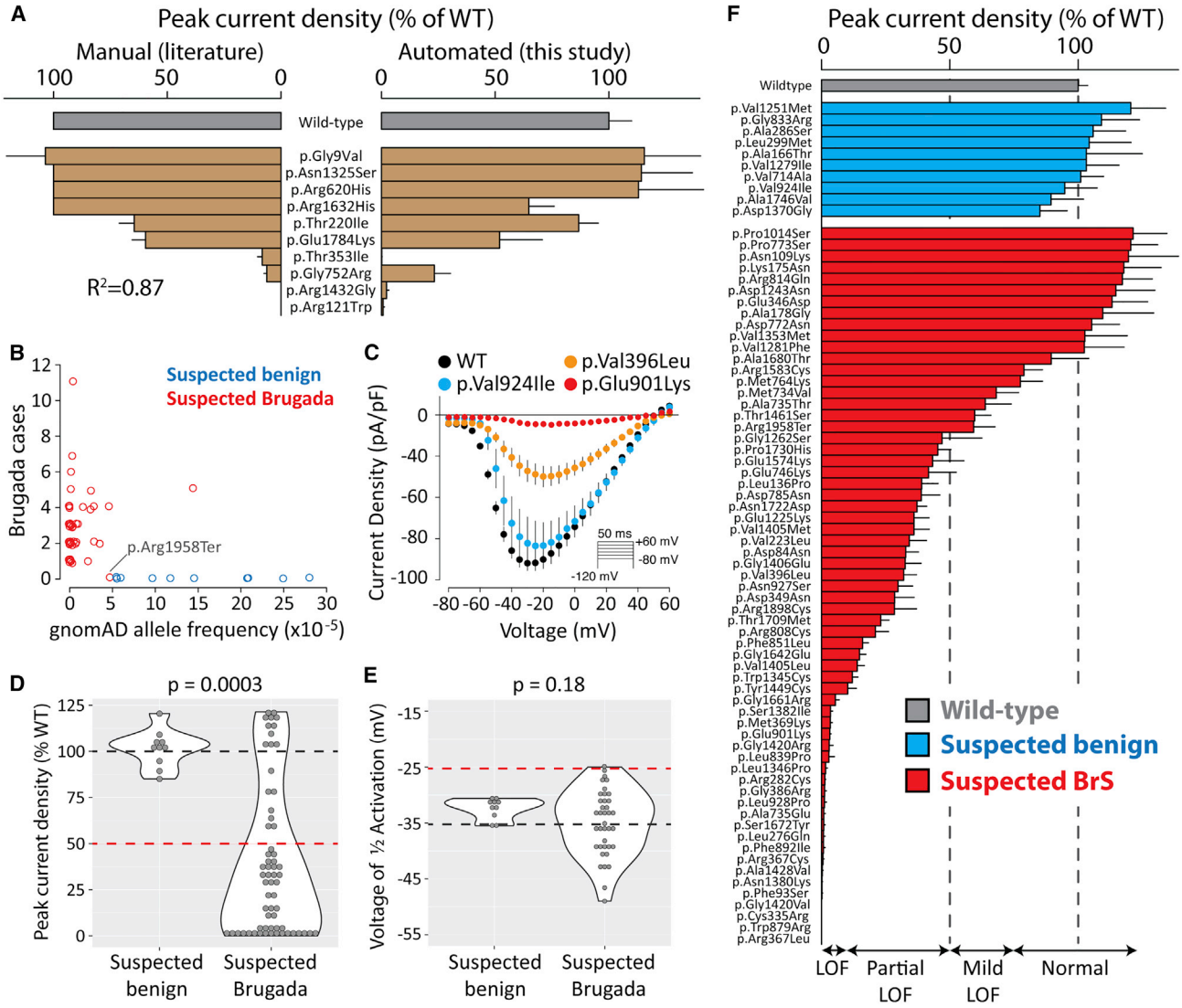

Figure 2. Suspected Brugada Syndrome Variants Have Reduced Peak Current

(A) Peak current density of ten variants previously studied by manual patch clamp. Mean ± standard errors. Left: literature values. For some variants, standard errors were not reported. Right: automated patch clamp values (this study).

(B) Selection of suspected benign and suspected BrS-associated variants. Each data point is a variant. Points were "jittered" in the x and y axes with a small random number so that points with identical values would be visible. The x axis is the minor allele frequency in the gnomAD database. The y axis indicates the number of individuals with Brugada syndrome in the literature.[10] Values are taken from a recent collation of *SCN5A* data from the literature.[10] p.Arg1958Ter was classified as a suspected BrS variant because it is a nonsense variant, even though it has not been observed in any cases of BrS.

(C) Current-voltage curves for selected variants, showing an example of a normal variant (p.Val924Ile), a partial loss-of-function variant (p.Val396Leu), and a loss-of-function variant (p.Glu901Lys). Error bars indicate standard error of the mean.

(D and E) Violin plots comparing peak current density (D) or voltage of 1/2 activation (E) for suspected Brugada syndrome versus suspected benign variants. Wild-type values are indicated with a dashed black line, and cutoffs for deleteriousness are indicated with a red line (50% peak current or 10 mV rightward shift in $V_{1/2}$ activation). p values are from a two-tailed Mann-Whitney U test. For a complete list of measured parameters, see Table S7 and Data S1.

(F) Peak current density (normalized to wild-type) for all previously unstudied variants. Error bar indicates standard error of the mean.

We also conducted experiments to assess the effects of incubation at low temperature or mexiletine (a sodium channel blocker), interventions reported to increase cell surface expression of mistrafficked channels.[27–31] For these experiments, cells stably expressing loss-of-function variants were generated as described above. The cells were incubated for 24 h at 30°C, or at 37°C with or without 500 μM mexiletine hydrochloride (Sigma), washed with HEK media, and were patch clamped as described above.

Data Analysis

Cells with a seal resistance of 0.5–10 GΩ and a cell capacitance between 5 and 30 pF were analyzed. Built-in SyncroPatch windowing methods were used to calculate currents in peak/inactivation/recovery from inactivation protocols (maximum current from 0.5 to 5 ms post voltage shift) or late current (mean current from 190 to 200 ms). These values were exported to .csv files and analyzed in custom R scripts. Current-voltage plots were created for each well, and each well was manually analyzed and classified

as normal/in voltage control (voltage-dependent current with peak current near −20 mV), out of voltage control (voltage-dependent current that rapidly jumped around −60 mV), or having no current (<25 pA peak current). Example current-voltage curves of these three classes are shown in Figure S3.

Only wells that were in voltage control (Figure S3) with peak currents between 100 and 2,000 pA were used to assess additional features, such as the voltage dependence of activation, voltage dependence of inactivation, inactivation time, or recovery from inactivation (Table S4). Additional details on peak current averaging are presented in the Supplemental Methods. Only wells with a peak current above 500 pA and wells where the seal resistance and capacitance did not change by more than 10% during addition of tetracaine (see below) were used to measure late current. Activation and inactivation best-fit curves were calculated for each well by fitting Boltzmann equations using the R function *nls* (nonlinear least-squares). Recovery from inactivation data and inactivation time data were fitted with exponential curves with the *nls* function. Wells with high noise for which the best-fit curve did not fit the data well (data points had >10% average deviation from the best-fit line) were removed from the analysis. Tetracaine-sensitive late current was calculated as the mean of 5 post-tetracaine raw late current values subtracted from the mean of 5 pre-tetracaine values and was normalized to tetracaine-sensitive peak current. Outlier values exceeding 3 standard deviations from the mean were excluded (1.5% of all values, Table S4). Per-well $V_{1/2}$ activation (voltage at which half the channels are activated), $V_{1/2}$ inactivation (voltage at which half the channels are inactivated), time of 50% recovery from inactivation, inactivation time constant, and late current parameters were averaged across all wells meeting the above inclusion criteria. All measured parameters with at least 5 cells meeting inclusion criteria are reported. For many severe loss-of-function variants, there were fewer than 5 qualifying wells to accurately quantify channel parameters other than peak current density. All comparisons of variant parameters between groups were made in R with two-tailed t tests (*t.test*) or with two-tailed Mann-Whitney U tests (*wilcox.test* with the parameter paired = FALSE) when the distributions were non-normally distributed. Differences in dispersion between groups were tested with Levene's Test (*levene.test*, *car* package). Violin plots were made with *geom_violin* (ggplot2).

Variants were classified according to American College of Medical Genetics and Genomics (ACMG) criteria (Figure S4).[19] A custom R script was used to implement these criteria. Variant classifications pre- and post-functional data are presented in Table S1. A cutoff of 6/~250,000 alleles in gnomAD v.2.1[23] was used to determine criteria BS1 and PM2, following a previous recommended cutoff for Brugada syndrome.[32] BP4 and PP3 were determined from the consensus of PROVEAN[33] and PolyPhen2[34] classifications. PS4 was interpreted to mean at least 5 observed individuals with Brugada syndrome and an estimated Brugada syndrome penetrance from literature reports whose 95% confidence interval excluded 0.[10] Variants with peak current densities between 75% and 125% of wild-type, <10 mV shifts in activation or inactivation, <2-fold shifts in recovery from inactivation, and <1% late current (% of peak) were considered to have normal *in vitro* functional data (BS3). Variants with peak current densities <50% of wild-type or a >10 mV rightward shift in $V_{1/2}$ activation were considered to have abnormal loss-of-function functional data (PS3). Variants with >75% peak current and a late current >1% (normalized to peak current) were considered to have abnormal gain-of-function functional data (PS3). These cutoffs were determined from a previous analysis of the correlation between functional parameters and Brugada syndrome and long QT syndrome risk.[10] These cutoffs reflect the observation that variants that are not linked to disease often have mild perturbations to their patch clamp parameters. ClinVar classifications[35] were used to determine criteria BP6 and PP5. All literature and gnomAD case/control counts, peak current densities, and classifications pre- and post-patch clamp data are presented in Table S1, and ACMG criteria used for variant classification are presented in Table S5. All variants were considered to meet PP2 (missense variant in gene with low rate of benign missense variants and pathogenic missense variants common) except p.Arg1958Ter, which was considered to meet PM4 (protein length changing variant). For gnomAD counts, literature counts, and classifications, variants with the same outcome on the protein sequence (due to the redundant genetic code) were grouped together. Therefore, the PS1 criterion (same amino acid change as established pathogenic variant) was not used. No variants satisfied the PP1 criterion (statistical co-segregation with disease in multiple affected family members) due to the low numbers of carriers in the literature and lack of large published pedigrees for these variants. We performed an initial round of classification without using PM5 (missense variant at a position where a different variant is pathogenic/likely pathogenic). Then, for each variant, we determined the PM5 criterion by searching for variants at the same amino acid position that were initially classified as pathogenic/likely pathogenic. Finally, classifications were recalculated including PM5.

Homology Model and Structural Calculations

All computational modeling was conducted in parallel to and blinded from the experimental characterizations. Structural models of human *SCN5A* (UniProtKB: Q14524-1, modeled residues: 30–440, 685–957, 1174–1887) bound with *SCN1B* (UniProtKB: Q07699-1, modeled residues: 20–192) were generated by homology modeling using the protein structure prediction software Rosetta (v.3.10).[36] The cryo-EM structure of human *SCN9A* bound with *SCN1B* and the Ig domain of *SCN2B* resolved to 3.2 Å (PDB: 6J8H)[37] was used as the primary template while the cryo-EM structure of NavPaS from American Cockroach resolved to 2.6 Å (PDB: 6A95)[38] was used as a secondary template. The percent identity between the aligned positions of *SCN9A* and *SCN5A* sequences was 76.7%. While the percent identity between NavPaS and *SCN5A* was only moderate (45.6%), the N-terminal and C-terminal domains in the NavPaS structure were partially resolved, providing coordinates for modeling the corresponding domains of *SCN5A*. The final model (Figures 4 and S5) covers 70 of the 73 functionally characterized variants. Three variants—p.Pro1014Ser, p.Arg1898Cys, and p.Arg1958Ter—fall outside of the set of modeled residues, and are therefore not covered. Additional information about the homology model and ΔΔG (thermostability) calculations are presented in the Supplemental Methods and Table S6.

Results

Automated Patch Clamping of $Na_V1.5$ Variants

Across multiple transfections and variants, a high percentage (85.4% ± 12.3% SEM) of HEK293 cells were mCherry positive, indicating successful integration of an *SCN5A* expression plasmid (Figures 1A and S1). Wild-type and

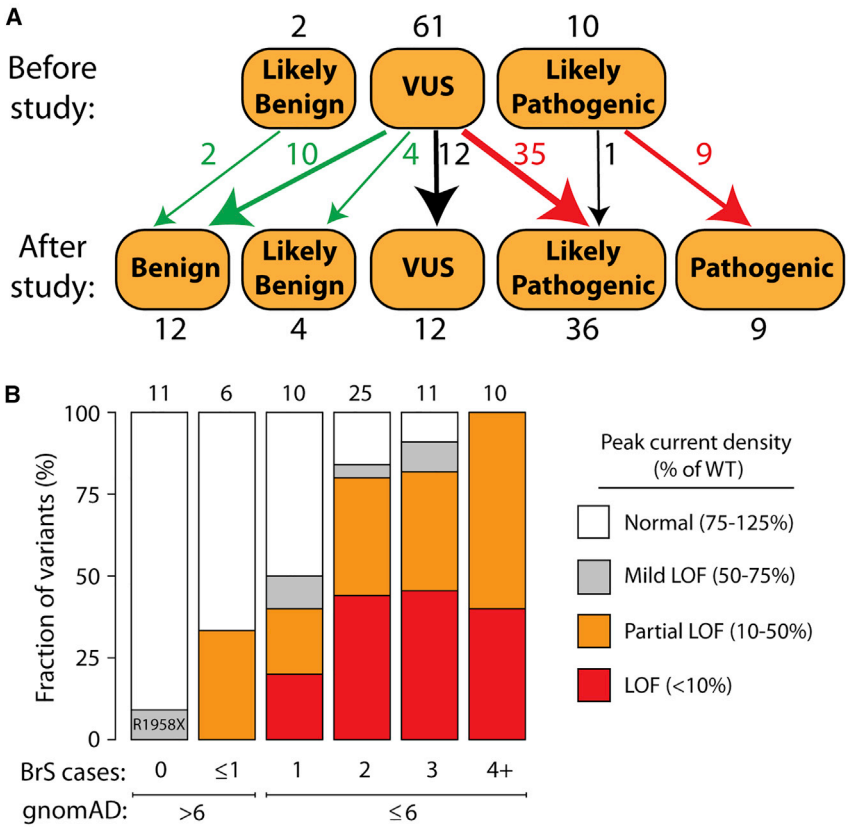

Figure 3. Reclassifications with Patch Clamp Data

(A) Variants were classified according to the American College of Medical Genetics and Genomics criteria.[19] Above: classifications before the patch clamp data in this study. Below: classifications with the patch clamp data in this study. All classifications indicate Brugada syndrome, except for p.Arg814Gln, which was reclassified from likely pathogenic for Brugada syndrome to likely pathogenic for long QT syndrome.

(B) Patch clamp results varied depending on the number of observed individuals with Brugada syndrome in the literature[10,18] and the gnomAD allele frequency.[23] LoF, loss of function.

mutant cells were patch clamped with the SyncroPatch 384PE device (Figure 1). For cells expressing wild-type *SCN5A*, most wells that passed seal resistance and capacitance quality control cutoffs had voltage-dependent sodium currents (86.9% ± 14.6% SEM, Figures 1B and 1C). Wild-type cells had typical $Na_V1.5$ properties (Figures 1 and S2).

To validate the automated patch clamping method, we patch clamped 10 previously studied variants chosen because they had a range of functional properties. The previously published manual patch clamp properties were concordant with the automated patch clamp data (Figure 2A, Table S7). Peak current is the major parameter of interest for assessing Brugada syndrome risk.[10] We observed a strong correlation ($R^2 = 0.87$) between the automated peak current density measurements and previously published manual patch clamp peak current density values (Figure 2A). p.Arg1632His and p.Gly752Arg had differences in peak current compared to previous manual patch clamp data (65% peak current density versus no reported difference from wild-type for p.Arg1632His;[39] 23% peak current density versus 6% previously reported for p.Gly752Arg[40]). These differences might represent differences in cell lines,[40] differences in data analysis pipelines, or experimental measurement error inherent in these measurements. These two variants had previously published changes to other properties[39,40] that were recapitulated by automatic patch clamping (a dramatic increase in time to recover from inactivation for p.Arg1632His [Figure S9] and a right-shift in activation voltage for p.Gly752Arg [Figure S6]).

From our previous curation of the *SCN5A* variant literature,[10] we selected 73 previously unstudied variants: 63 suspected Brugada syndrome variants and 10 suspected benign variants. The suspected benign and suspected Brugada syndrome variants were selected based on their frequency in the gnomAD database and in the literature in individuals with Brugada syndrome (Figure 2B, Table S1).[10,23] Applying ACMG classification criteria, without patch clamping data, 61 variants were classified as VUS, 2 as likely benign, and 10 as likely pathogenic (Figure 3A, Table S1).

Most Suspected Brugada Syndrome Variants Had (Partial) Loss of Function

There was a striking difference in peak current density between the suspected BrS and suspected benign variants ($p = 0.0003$, two-tailed Mann-Whitney U test, Figure 2D). Overall, 23/63 suspected BrS variants had partial loss of function (10%–50% peak current density, normalized to wild-type) and 22/63 had loss of function (<10%), while 10/10 suspected benign variants had normal peak currents (75%–125%) (Figure 2F, Table 1). We next examined whether large changes to other parameters were a common cause of channel loss of function. There was a statistically significant increase in width of the distribution of $V_{1/2}$ activations in the suspected BrS set ($p = 0.0028$, Levene's test). However, only 2/39 variants with measured $V_{1/2}$ activation had a >10 mV rightward shift (WT: −36.7 ± 0.6 mV, n = 279; D785N: −26.4 ± 1.3 mV, n = 16; D349N: −26.5 ± 3.1 mV, n = 5). p.Asp785Asn and p.Asp349Asn both also had a partial loss of function in peak current (38.9% and 28.5% of WT, respectively; Figure 2F). One suspected BrS variant, p.Gly1262Ser, had a combination of a partial loss of function of peak current density (47% of wild-type) and a gain of function

Table 1. Functional Class of Suspected Benign and Brugada Syndrome Variants

Functional Class	Peak Current Density	Suspected Benign	Suspected BrS
Normal	75%–125%	10 (100%)	14 (22%)
Mild loss of function	50%–75%	0 (0%)	4 (6%)
Partial loss of function	10%–50%	0 (0%)	23 (37%)
Loss of function	<10%	0 (0%)	22 (35%)
Total	*	10	63

leftward shift in $V_{1/2}$ activation (−12.2 mV; Figure S6). Overall, there was no significant difference in $V_{1/2}$ activation between suspected BrS and suspected benign variants ($p = 0.18$, Mann-Whitney U test, Figure 2E). Therefore, in this dataset, large shifts in activation gating were not a common cause of Brugada syndrome. Surprisingly, one suspected BrS-associated variant, p.Arg814Gln, had near wild-type-like peak current density (117% of wild-type) and increased late current (1.4% of peak). In addition to Brugada syndrome cases, p.Arg814Gln has been observed in two cases of long QT syndrome,[41] consistent with its gain-of-function late current phenotype. Besides these variants, no major differences between suspected BrS and suspected benign variants were observed for $V_{1/2}$ inactivation, inactivation time, recovery from inactivation, or late current (Figures S6–10, Table S7). Despite being a nonsense variant, p.Arg1958Ter generated substantial current (peak current density of 59.3% of wild-type), likely due to the fact that the stop codon is in the distal C terminus of the protein (Figure 2F).

Some suspected BrS variants have only been observed in only a single individual with BrS, whereas other variants have been observed in multiple individuals. In this study, the patch clamp phenotypes varied according to the strength of the phenotypic evidence for Brugada syndrome (Figure 3B). For example, 4/10 variants that have been observed in exactly 1 case of Brugada syndrome and ≤6 in gnomAD had partial or complete loss of function (0%–50% peak current). In contrast, 10/10 variants that have been observed in at least 4 BrS1 cases and ≤6 in gnomAD had partial or complete loss of function. 2/6 variants seen in ≥1 cases of Brugada syndrome but also in >6 counts in gnomAD had partial loss-of-function defects. Therefore, variants that were more commonly observed in Brugada syndrome cases and less frequently observed in the population were more likely to have loss of channel function.

Reclassification of Variants with Functional Data

When we implemented the ACMG classification criteria[19] to classify all studied variants without the automated patch clamp data (Figure 3A), 60/73 variants were classified as VUS. Based on our previous literature curation study, which showed an elevated BrS risk for variants with peak current density <50% of wild-type,[10] we defined cutoffs for ACMG functional criteria PS3 and BS3. Variants with <50% peak current were considered to meet criterion PS3 (well-established functional assays show a change), and variants with 75%–125% peak current were considered to meet criterion BS3 (well-established functional assays show no change). Since the phenotypic consequences of mild LoF variants (50%–75% peak current) to BrS risk is unclear,[10] these variants were not considered to satisfy either PS3 or BS3. Because of its elevated late current and normal peak current, p.Arg814Gln was considered to meet the PS3 criterion for abnormal gain of function, and was reclassified from likely pathogenic for Brugada syndrome to likely pathogenic for long QT syndrome. p.Gly1262Ser, which had peak current density of 47% of wild-type and a gain of function 12.2 mV leftward shift in $V_{1/2}$ activation, was considered to meet neither the PS3 nor the BS3 criteria because of the uncertain impact of these features on BrS risk. After patch clamping data were incorporated, 36/61 VUSs were reclassified as likely pathogenic and 14 were reclassified as likely benign or benign. Overall, classifications were changed for 49/61 VUSs (80%) and 61/73 (84%) previously unstudied variants. Therefore, for this set of variants, functional data led to reclassification of the great majority of VUSs.

Partial Rescue of Some Loss-of-Function Variants

Previous studies have shown that pre-incubation of cells at a lower temperature or with a sodium channel blocker can partially rescue the function of some loss-of-function *SCN5A* variants, typically by improving protein folding and trafficking to the cell surface.[27,29–31] Therefore, we tested whether pre-incubating cells at 30°C or with the sodium channel blocker mexiletine could partially rescue sodium current for the 22 loss-of-function variants (<10% normalized peak current density). Cells expressing these variants were cultured for 24 h in usual conditions at 37° with no added drug, at 30°C, or with 500 μM mexiletine. Compared to usual conditions, 8/22 variants had significantly increased peak current at 30°C and 2/22 variants had significantly increased peak current when treated with mexiletine (Figure S11). p.Phe892Ile and p.Met369Lys had the largest responses to 30°C incubation, with normalized peak current density increasing from 8.7% at 37°C to 34.8% at 30°C for p.Phe892Ile ($p = 0.006$, two-tailed t test) and from 3.9% to 42.5% for p.Met369Lys ($p = 0.0003$; Figure S11).

Structural Basis of Loss of Function

In this study, 22 previously unstudied variants had <10% peak current and an additional 23 variants had 10%–50%

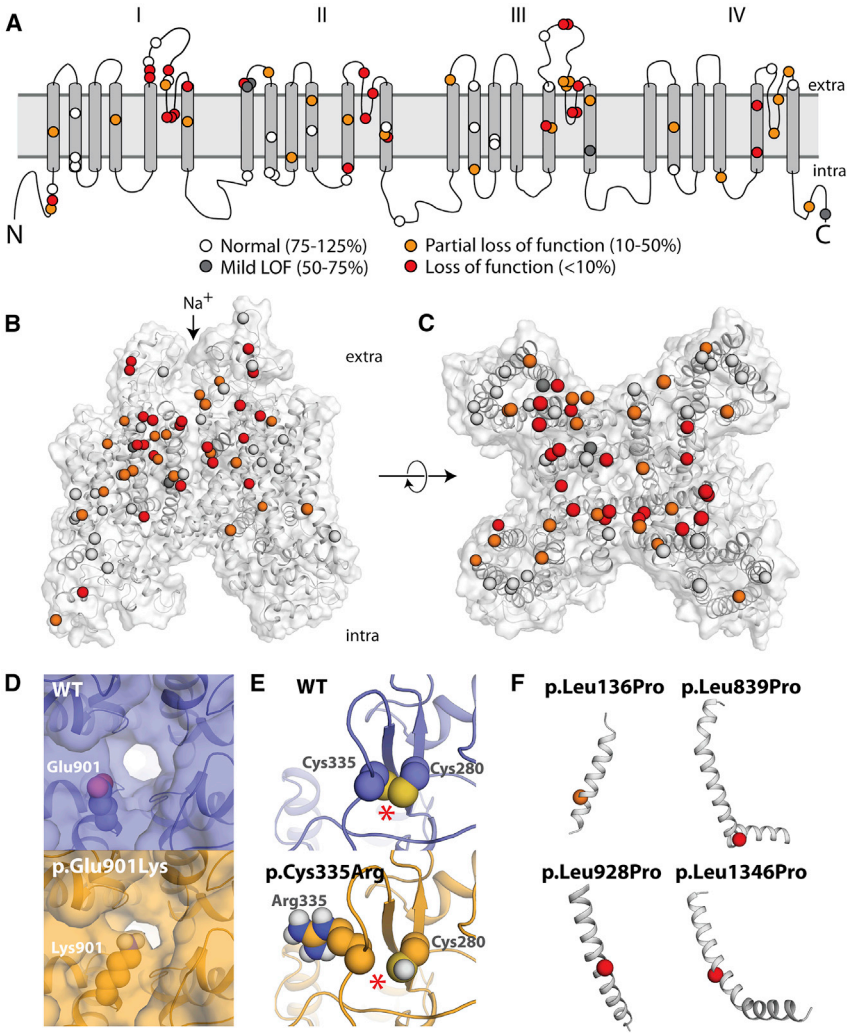

Figure 4. Structural Basis of *SCN5A* Loss-of-Function Variants

(A) Two-dimensional schematic of $Na_V1.5$ structure. All previously unstudied variants are shown and color-coded based on peak current density (white 75%–125%, gray 50%–75%, orange 10%–50%, red < 10%).

(B and C) Three-dimensional homology model of $Na_V1.5$. Variants are colored as in (A).

(D) Top-down view of WT (top) and p.Glu901Lys (bottom), as modeled using Rosetta. The lysine residue projects into the pore, likely disrupting sodium passage.

(E) View of WT and p.Cys335Arg, as modeled using Rosetta. The WT protein has a disulfide bond between Cys335 (left) and Cys280 (right), which was inferred from the spatial proximity of these two residues and the fact that the corresponding residues in the template structures also form a disulfide bond; this bond is disrupted by p.Cys335Arg. The disulfide bond is indicated with an asterisk (*).

(F) Four leucine -> proline variants in this study. p.Leu136Pro is a partial loss-of-function variant and p.Leu839P, p.Leu928Pro, and p.Leu1340Pro are loss of function. The structures of these four variants were not modeled because modeling drastic structural changes involving prolines that are part of a helix usually cannot be reliably modeled in Rosetta. However, these variants likely cause loss of protein function by causing a kink in the alpha helix and protein misfolding.

current. We explored the structural basis of these variants' decreased channel function. Although the suspected BrS variants were selected for study independent of their position in the protein, 42/45 (partial) loss-of-function variants were located in the four structured transmembrane domains, as opposed to unstructured linker regions or the N and C termini (Figures 4A–4C). 33/45 (73%) loss/partial loss-of-function variants were located in the pore-forming or pore-adjacent S5, S5-S6 linker, or S6 regions, areas that we have previously identified as a hotspot for Brugada variants.[10,17] Indeed, variant distance from the pore in the protein structure was strongly correlated with normalized peak current density (Pearson's r = 0.54, p = 1.3e–6, Figure S12).

Many disease-causing variants cause amino acid substitutions that lead to a significant perturbation to native thermostability (|ΔΔG|) of protein structure.[42,43] To investigate the extent to which the perturbation to the native thermostability of $Na_V1.5$ is correlated with molecular function, we evaluated the impact of each variant on estimated thermostability relative to the wild-type structure with a Rosetta ΔΔG protocol.[44] Normalized peak currents and estimated |ΔΔG| values were significantly negatively correlated (Pearson's r = −0.31, p = 0.0092, Figure S13). The estimated |ΔΔG| of variants with functional effects on peak current (peak current density < 50%, n = 44, median |ΔΔG| = 2.00 kcal/mol) was significantly larger than normal/mild loss-of-function variants (peak current density ≥ 50%, n = 26, median |ΔΔG| = 0.88 kcal/mol, Mann-Whitney U test, p = 0.0031, Figure S13B). This result suggests that variant-induced disruption of native thermostability of $Na_V1.5$ may be a major factor contributing to compromised function.

Variants can cause complete or partial loss of function through mechanisms other than affecting thermostability, such as disrupting the native topology or electrostatic environment of the pore. Using a homology model of $Na_V1.5$, several variants had plausible mechanisms that could explain their loss-of-function phenotype (Figures 4D–4F). Seven pore-lining residues in this study, p.Asp349Asn, p.Arg367Cys, p.Arg367Leu, p.Trp879Arg, p.Phe892Ile, p.Glu901Lys, and p.Thr1709Met, caused either complete or partial loss of function while inducing negligible or only minor perturbations to native thermostability

(Figures 4C, 4D, and S14). In particular, the residue Glu901 lines the channel pore, and in the homology model, the loss-of-function variant p.Glu901Lys projects into the pore, likely disrupting sodium permeation (Figure 4D). p.Cys335Arg disrupts a disulfide bond, likely destabilizing the tertiary structure of the protein and explaining its loss-of-function phenotype (Figure 4E). Three loss-of-function leucine→proline variants (p.Leu839Pro, p.Leu928Pro, and p.Leu1346Pro) and a fourth partial loss-of-function variant (p.Leu136Pro) likely disrupt alpha helices, as is seen in other proteins with proline variants (Figure 4F).[45] In contrast, p.Ala166Thr, a suspected benign variant located distally from the pore and not predicted to alter protein structure, had wild-type-like electrophysiological properties (Figures S5B and S5C, Table S1). These data indicate that structural features can help predict or explain channel loss of function in *SCN5A* variants.

Discussion

Reclassification of Brugada Syndrome Variants with Patch Clamping Data

This study identified 44 novel (partial) loss-of-function variants by high-throughput, automated patch clamping. In addition, this nearly doubles (from 24 to 46) the number of known loss-of-function missense *SCN5A* variants with <10% peak current (Table S8). As a result of the patch clamp data, 35 novel pathogenic/likely pathogenic variants and 14 novel benign/likely benign variants were identified. Overall, 61/73 variants, including 49/61 VUSs, were reclassified with our patch clamp data. A nonsense variant, p.Arg1958Ter, has been observed in 13 individuals in the gnomAD database and never in a published case of Brugada syndrome. p.Arg1958Ter generated substantial current (peak current density of 59.3% of wild-type) and likely escapes nonsense-mediated decay because it located is in the last exon of *SCN5A*. p.Arg1958Ter was not considered to meet the PVS1 criterion (null variant) and was classified as a VUS both pre- and post-study due to its mild loss-of-function *in vitro* phenotype. Eight other nonsense and frameshift variants in the C terminus of *SCN5A* are present in the gnomAD database;[23] these variants may also generate sodium current and not have complete loss of channel function.

A recent guide from the ClinGen consortium recommended that *in vitro* assays that are well validated with clearly pathogenic and benign controls and predict disease risk well be used as PS3/BS3 at the strong level in the ACMG classification scheme.[46] Since patch clamping is the gold standard method to assay ion channel function and has been performed for hundreds of *SCN5A* variants including (for the most part) correctly predicting the phenotypic impact of dozens of clearly benign and pathogenic variants, we implemented the PS3 and BS3 criteria at the strong level for variants between 0%–50% peak current density (PS3) and 75%–125% (BS3). These ranges were chosen based on the correlation between peak current and variant-specific BrS risk.[10] Because of their uncertain impact on Brugada syndrome risk, mild loss-of-function variants (50%–75% peak current) were not considered to meet BS3 or PS3. As a result, the classification of these variants was not changed due to this study.

While each variant is rare, the collective allele frequency of the reclassified variants in this study is 0.2% in gnomAD (~0.4% of individuals). Although the majority of the 1,390 observed *SCN5A* missense variants remain VUSs,[10] this study suggests that variant properties can be used to identify a subset of *SCN5A* variants that are highly enriched for altered *in vitro* properties and disease association. In this study, two properties predict a high rate of *in vitro* loss of function: (1) the observation of the variant in at least one individual with BrS and (2) ultra-rare frequency in the population (≤6 in gnomAD—concordant with a previous computational estimate[32]). Including this study, 135 of the 276 variants with these properties have been now studied *in vitro*. The remaining 141 variants are excellent candidates for future high-throughput functional characterization and possible reclassification. An important open question is the rate of deleterious *in vitro* phenotypes in the 742 ultra-rare variants (≤6 in gnomAD) that have not been observed in any BrS cases to date. Some of these variants might not have appeared in published BrS cases despite a true BrS risk, or carriers may present with other *SCN5A*-associated arrhythmia phenotypes.[47]

It is important to note that *SCN5A* variant classification does not completely predict Brugada syndrome risk in individual patients. BrS is an incompletely penetrant disease, and its presentation is influenced by demographic factors such as age and sex,[48] as well as common genetic variants—including multiple noncoding haplotypes near *SCN5A*.[49] Individuals with loss-of-function *SCN5A* variants can present with other arrhythmias besides Brugada syndrome, including sick sinus syndrome,[5] atrial standstill,[50] or other conduction disease.[51] Therefore, carriers of the loss-of-function variants identified in this study may present with those conditions instead of Brugada syndrome. In addition, some "overlap" *SCN5A* variants can have increased risk of both Brugada syndrome and long QT syndrome.[52] One suspected BrS-associated variant in this study, p.Arg814Gln, had late current above our cutoff (>1% of peak current) and has appeared in the literature in both BrS and LQT cases.[41,53] Carriers of incidental pathogenic or likely pathogenic *SCN5A* variants should have follow-up ECG screening and a clinical and family history taken to determine each individual's phenotype and sudden cardiac death risk. A common variant in *SCN5A*, p.His558Arg, is present at a minor allele frequency of 22.3% in the gnomAD database.[23] This variant has been shown to modulate the effect of some *SCN5A* variants, although there is still a strong correlation between variant properties in the His558 and Arg558 backgrounds.[54] Future work will investigate the role of the Arg558 background on the variants in this study, which may enable more precise predictions of disease risk from *SCN5A* genotype.

Mechanisms of $Na_V1.5$ Loss of Function

In this set of variants, the most common cause of channel loss of function was a partial or total reduction in peak current. This is consistent with previous clamp studies[13–15] and our previous literature analysis which found that *SCN5A* peak current was the largest single predictor of Brugada syndrome risk.[10] Two variants, p.Asp785Asn and p.Asp349Asn, had a >10 mV rightward shift in $V_{1/2}$ activation; however, these two variants also had <50% peak current. Thus, while variants with large gating defects have been previously described (e.g., p.Arg1632His[39]), the major mechanism of $Na_V1.5$ loss of function is a reduction in peak current. Previous studies have found that channel misfolding and a resulting cell-surface trafficking deficiency is a common mechanism of loss-of-function variants in *SCN5A*[5,27] and other ion channel genes.[55] We observed a negative correlation between peak current density and computationally predicted |ΔΔG|, an estimate of variant-induced perturbations to native thermostability, consistent with other studies that showed that thermostability perturbations are a major cause of altered protein function.[56–59] In addition, structural modeling identified several probable modes of channel dysfunction, including pore-lining variants that likely disrupt sodium permeation, removal of a disulfide bond, or creation of prolines that likely disrupt alpha helices. Although these structural analyses were enlightening, structural features do not yet fully predict channel function, highlighting the complementarity of structural modeling and empirical electrophysiological measurements. Consistent with previous studies of *SCN5A* variants,[27–31] some but not all (8/22) *SCN5A* loss-of-function variants were partially rescued by 30° treatment or mexiletine. Although these treatments are not practical in the clinic for treatment of Brugada syndrome, this result suggests that other drugs or interventions may help rescue some *SCN5A* loss-of-function variants.

High-Throughput Approaches to Variant Classification

High-throughput patch clamping is a promising method for reclassifying the thousands of variants of uncertain significance in Mendelian arrhythmia genes. Previously, Vanoye et al.[22] reclassified 23/35 "uninformative" *KCNQ1* variants (variants of uncertain significance, variants with conflicting interpretations, or no available data). Ng et al.[21] reclassified 13 uninformative variants in *KCNH2* with patch clamping and cell surface abundance assays. This work combines high-throughput patch clamping and structural modeling, and explicitly incorporates ACMG classification criteria to reclassify 49/61 *SCN5A* VUSs, 35 to likely pathogenic, and 14 to benign/likely benign. Our approach may be extended to study additional *SCN5A* variants, including gain-of-function long QT-associated variants or additional variants observed in population sequencing efforts. Accurate classification of the large number of variants in arrhythmia-associated genes will require integrating data from multiple different model systems, such as patch clamping,[21,22] induced pluripotent stem cell-derived cardiomyocytes,[60–62] structural and computational models,[17,63,64] and ultra-high-throughput multiplexed assays.[65–67]

Limitations

This study assays variants in a heterologous expression system. While peak current as measured in this system is the strongest available *in vitro* predictor of Brugada syndrome risk,[10] it is possible for some variants to show different properties in HEK293T cells compared to cardiomyocytes, e.g., because of other proteins that interact with or modify $Na_V1.5$.[68–70] This study examined only the most common haplotype (H558) and the most common cardiac splice isoform of *SCN5A*; for some variants, it has been shown that alternate haplotypes/isoforms can modulate channel properties.[54]

Conclusion

This study used automated patch clamping to study 73 previously unstudied *SCN5A* variants, resulting in the reclassification of 49/61 variants of uncertain significance. This approach can help reclassify variants in this important disease gene and improve the accuracy and scope of genetic medicine.

Data and Code Availability

Additional data and code from this study is available upon reasonable request from the corresponding author.

Supplemental Data

Supplemental Data can be found online at https://doi.org/10.1016/j.ajhg.2020.05.015.

Acknowledgments

We thank Kenneth Matreyek and Douglas Fowler for sharing HEK293 cell lines and Tim Strassmaier and Carlos Vanoye for helpful advice. The Nanion SyncroPatch 384PE is housed and managed within the Vanderbilt High-Throughput Screening center, an institutionally supported core, and was funded by NIH Shared Instrumentation Grant 1S10OD025281. This research was funded by NIH grants K99 HG010904 (A.M.G.), K99 HL135442 (B.M.K.), R01 HL149826 (D.M.R.), and P50 GM115305 (D.M.R.) and American Heart Association fellowships 20POST35220002 (B.L.) and 20PRE35180088 (A.M.).

Declaration of Interests

The authors declare no competing interests.

Received: December 27, 2019
Accepted: May 19, 2020
Published: June 12, 2020

Web Resources

RCSB Protein Data Bank, http://www.rcsb.org/pdb/home/home.do

References

1. Kapplinger, J.D., Tester, D.J., Alders, M., Benito, B., Berthet, M., Brugada, J., Brugada, P., Fressart, V., Guerchicoff, A., Harris-Kerr, C., et al. (2010). An international compendium of mutations in the SCN5A-encoded cardiac sodium channel in patients referred for Brugada syndrome genetic testing. Heart Rhythm *7*, 33–46.
2. Kapplinger, J.D., Tester, D.J., Salisbury, B.A., Carr, J.L., Harris-Kerr, C., Pollevick, G.D., Wilde, A.A.M., and Ackerman, M.J. (2009). Spectrum and prevalence of mutations from the first 2,500 consecutive unrelated patients referred for the FAMILION long QT syndrome genetic test. Heart Rhythm *6*, 1297–1303.
3. Moreau, A., Gosselin-Badaroudine, P., Delemotte, L., Klein, M.L., and Chahine, M. (2015). Gating pore currents are defects in common with two Nav1.5 mutations in patients with mixed arrhythmias and dilated cardiomyopathy. J. Gen. Physiol. *145*, 93–106.
4. Bezzina, C.R., Rook, M.B., Groenewegen, W.A., Herfst, L.J., van der Wal, A.C., Lam, J., Jongsma, H.J., Wilde, A.A., and Mannens, M.M. (2003). Compound heterozygosity for mutations (W156X and R225W) in SCN5A associated with severe cardiac conduction disturbances and degenerative changes in the conduction system. Circ. Res. *92*, 159–168.
5. Gui, J., Wang, T., Jones, R.P., Trump, D., Zimmer, T., and Lei, M. (2010). Multiple loss-of-function mechanisms contribute to SCN5A-related familial sick sinus syndrome. PLoS ONE *5*, e10985.
6. Brugada, J., Campuzano, O., Arbelo, E., Sarquella-Brugada, G., and Brugada, R. (2018). Present Status of Brugada Syndrome: JACC State-of-the-Art Review. J. Am. Coll. Cardiol. *72*, 1046–1059.
7. Hosseini, S.M., Kim, R., Udupa, S., Costain, G., Jobling, R., Liston, E., Jamal, S.M., Szybowska, M., Morel, C.F., Bowdin, S., et al.; National Institutes of Health Clinical Genome Resource Consortium (2018). Reappraisal of Reported Genes for Sudden Arrhythmic Death: Evidence-Based Evaluation of Gene Validity for Brugada Syndrome. Circulation *138*, 1195–1205.
8. Brugada, P., and Brugada, J. (1992). Right bundle branch block, persistent ST segment elevation and sudden cardiac death: a distinct clinical and electrocardiographic syndrome. A multicenter report. J. Am. Coll. Cardiol. *20*, 1391–1396.
9. Milman, A., Andorin, A., Postema, P.G., Gourraud, J.B., Sacher, F., Mabo, P., Kim, S.H., Maeda, S., Takahashi, Y., Kamakura, T., et al. (2019). Ethnic differences in patients with Brugada syndrome and arrhythmic events: New insights from Survey on Arrhythmic Events in Brugada Syndrome. Heart Rhythm *16*, 1468–1474.
10. Kroncke, B.M., Glazer, A.M., Smith, D.K., Blume, J.D., and Roden, D.M. (2018). *SCN5A* ($Na_V1.5$) Variant Functional Perturbation and Clinical Presentation: Variants of a Certain Significance. Circ Genom Precis Med *11*, e002095.
11. Wang, D.W., Yazawa, K., George, A.L., Jr., and Bennett, P.B. (1996). Characterization of human cardiac Na+ channel mutations in the congenital long QT syndrome. Proc. Natl. Acad. Sci. USA *93*, 13200–13205.
12. Kalia, S.S., Adelman, K., Bale, S.J., Chung, W.K., Eng, C., Evans, J.P., Herman, G.E., Hufnagel, S.B., Klein, T.E., Korf, B.R., et al. (2017). Recommendations for reporting of secondary findings in clinical exome and genome sequencing, 2016 update (ACMG SF v2.0): a policy statement of the American College of Medical Genetics and Genomics. Genet. Med. *19*, 249–255.
13. Chen, Q., Kirsch, G.E., Zhang, D., Brugada, R., Brugada, J., Brugada, P., Potenza, D., Moya, A., Borggrefe, M., Breithardt, G., et al. (1998). Genetic basis and molecular mechanism for idiopathic ventricular fibrillation. Nature *392*, 293–296.
14. Deschênes, I., Baroudi, G., Berthet, M., Barde, I., Chalvidan, T., Denjoy, I., Guicheney, P., and Chahine, M. (2000). Electrophysiological characterization of SCN5A mutations causing long QT (E1784K) and Brugada (R1512W and R1432G) syndromes. Cardiovasc. Res. *46*, 55–65.
15. Kapplinger, J.D., Giudicessi, J.R., Ye, D., Tester, D.J., Callis, T.E., Valdivia, C.R., Makielski, J.C., Wilde, A.A., and Ackerman, M.J. (2015). Enhanced Classification of Brugada Syndrome-Associated and Long-QT Syndrome-Associated Genetic Variants in the SCN5A-Encoded Na(v)1.5 Cardiac Sodium Channel. Circ Cardiovasc Genet *8*, 582–595.
16. Priori, S.G., Napolitano, C., Gasparini, M., Pappone, C., Della Bella, P., Giordano, U., Bloise, R., Giustetto, C., De Nardis, R., Grillo, M., et al. (2002). Natural history of Brugada syndrome: insights for risk stratification and management. Circulation *105*, 1342–1347.
17. Kroncke, B.M., Mendenhall, J., Smith, D.K., Sanders, C.R., Capra, J.A., George, A.L., Blume, J.D., Meiler, J., and Roden, D.M. (2019). Protein structure aids predicting functional perturbation of missense variants in *SCN5A* and *KCNQ1*. Comput. Struct. Biotechnol. J. *17*, 206–214.
18. Kroncke, B.M., Smith, D.K., Glazer, A.M., Roden, D.M., and Blume, J.D. (2019). A Bayesian method using sparse data to estimate penetrance of disease-associated genetic variants. bioRxiv. https://doi.org/10.1101/571158.
19. Richards, S., Aziz, N., Bale, S., Bick, D., Das, S., Gastier-Foster, J., Grody, W.W., Hegde, M., Lyon, E., Spector, E., et al.; ACMG Laboratory Quality Assurance Committee (2015). Standards and guidelines for the interpretation of sequence variants: a joint consensus recommendation of the American College of Medical Genetics and Genomics and the Association for Molecular Pathology. Genet. Med. *17*, 405–424.
20. Kang, S.K., Vanoye, C.G., Misra, S.N., Echevarria, D.M., Calhoun, J.D., O'Connor, J.B., Fabre, K.L., McKnight, D., Demmer, L., Goldenberg, P., et al. (2019). Spectrum of KV2.1 dysfunction in KCNB1-associated neurodevelopmental disorders. Ann. Neurol. *86*, 899–912.
21. Ng, C.A., Perry, M.D., Liang, W., Smith, N.J., Foo, B., Shrier, A., Lukacs, G.L., Hill, A.P., and Vandenberg, J.I. (2020). High-throughput phenotyping of heteromeric human ether-a-go-go-related gene potassium channel variants can discriminate pathogenic from rare benign variants. Heart Rhythm *17*, 492–500.
22. Vanoye, C.G., Desai, R.R., Fabre, K.L., Gallagher, S.L., Potet, F., DeKeyser, J.M., Macaya, D., Meiler, J., Sanders, C.R., and George, A.L., Jr. (2018). High-Throughput Functional Evaluation of KCNQ1 Decrypts Variants of Unknown Significance. Circ Genom Precis Med *11*, e002345.
23. Lek, M., Karczewski, K.J., Minikel, E.V., Samocha, K.E., Banks, E., Fennell, T., O'Donnell-Luria, A.H., Ware, J.S., Hill, A.J., Cummings, B.B., et al.; Exome Aggregation Consortium (2016). Analysis of protein-coding genetic variation in 60,706 humans. Nature *536*, 285–291.
24. Matreyek, K.A., Stephany, J.J., and Fowler, D.M. (2017). A platform for functional assessment of large variant libraries in mammalian cells. Nucleic Acids Res. *45*, e102.

25. Matreyek, K.A., Stephany, J.J., Chiasson, M.A., Hasle, N., and Fowler, D.M. (2020). An Improved Platform for Functional Assessment of Large Protein Libraries in Mammalian Cells. Nucleic Acids Res. *48*, e1.
26. Hermann, M., Stillhard, P., Wildner, H., Seruggia, D., Kapp, V., Sánchez-Iranzo, H., Mercader, N., Montoliu, L., Zeilhofer, H.U., and Pelczar, P. (2014). Binary recombinase systems for high-resolution conditional mutagenesis. Nucleic Acids Res. *42*, 3894–3907.
27. Clatot, J., Ziyadeh-Isleem, A., Maugenre, S., Denjoy, I., Liu, H., Dilanian, G., Hatem, S.N., Deschênes, I., Coulombe, A., Guicheney, P., and Neyroud, N. (2012). Dominant-negative effect of SCN5A N-terminal mutations through the interaction of Na(v)1.5 α-subunits. Cardiovasc. Res. *96*, 53–63.
28. Makiyama, T., Akao, M., Tsuji, K., Doi, T., Ohno, S., Takenaka, K., Kobori, A., Ninomiya, T., Yoshida, H., Takano, M., et al. (2005). High risk for bradyarrhythmic complications in patients with Brugada syndrome caused by SCN5A gene mutations. J. Am. Coll. Cardiol. *46*, 2100–2106.
29. Pfahnl, A.E., Viswanathan, P.C., Weiss, R., Shang, L.L., Sanyal, S., Shusterman, V., Kornblit, C., London, B., and Dudley, S.C., Jr. (2007). A sodium channel pore mutation causing Brugada syndrome. Heart Rhythm *4*, 46–53.
30. Valdivia, C.R., Ackerman, M.J., Tester, D.J., Wada, T., McCormack, J., Ye, B., and Makielski, J.C. (2002). A novel SCN5A arrhythmia mutation, M1766L, with expression defect rescued by mexiletine. Cardiovasc. Res. *55*, 279–289.
31. Valdivia, C.R., Tester, D.J., Rok, B.A., Porter, C.B., Munger, T.M., Jahangir, A., Makielski, J.C., and Ackerman, M.J. (2004). A trafficking defective, Brugada syndrome-causing SCN5A mutation rescued by drugs. Cardiovasc. Res. *62*, 53–62.
32. Whiffin, N., Minikel, E., Walsh, R., O'Donnell-Luria, A.H., Karczewski, K., Ing, A.Y., Barton, P.J.R., Funke, B., Cook, S.A., MacArthur, D., and Ware, J.S. (2017). Using high-resolution variant frequencies to empower clinical genome interpretation. Genet. Med. *19*, 1151–1158.
33. Choi, Y., and Chan, A.P. (2015). PROVEAN web server: a tool to predict the functional effect of amino acid substitutions and indels. Bioinformatics *31*, 2745–2747.
34. Adzhubei, I.A., Schmidt, S., Peshkin, L., Ramensky, V.E., Gerasimova, A., Bork, P., Kondrashov, A.S., and Sunyaev, S.R. (2010). A method and server for predicting damaging missense mutations. Nat. Methods *7*, 248–249.
35. Landrum, M.J., Lee, J.M., Benson, M., Brown, G., Chao, C., Chitipiralla, S., Gu, B., Hart, J., Hoffman, D., Hoover, J., et al. (2016). ClinVar: public archive of interpretations of clinically relevant variants. Nucleic Acids Res. *44* (D1), D862–D868.
36. Leaver-Fay, A., Tyka, M., Lewis, S.M., Lange, O.F., Thompson, J., Jacak, R., Kaufman, K., Renfrew, P.D., Smith, C.A., Sheffler, W., et al. (2011). ROSETTA3: an object-oriented software suite for the simulation and design of macromolecules. Methods Enzymol. *487*, 545–574.
37. Shen, H., Liu, D., Wu, K., Lei, J., and Yan, N. (2019). Structures of human $Na_v1.7$ channel in complex with auxiliary subunits and animal toxins. Science *363*, 1303–1308.
38. Shen, H., Li, Z., Jiang, Y., Pan, X., Wu, J., Cristofori-Armstrong, B., Smith, J.J., Chin, Y.K.Y., Lei, J., Zhou, Q., et al. (2018). Structural basis for the modulation of voltage-gated sodium channels by animal toxins. Science *362*, 362.
39. Benson, D.W., Wang, D.W., Dyment, M., Knilans, T.K., Fish, F.A., Strieper, M.J., Rhodes, T.H., and George, A.L., Jr. (2003). Congenital sick sinus syndrome caused by recessive mutations in the cardiac sodium channel gene (SCN5A). J. Clin. Invest. *112*, 1019–1028.
40. Potet, F., Mabo, P., Le Coq, G., Probst, V., Schott, J.J., Airaud, F., Guihard, G., Daubert, J.C., Escande, D., and Le Marec, H. (2003). Novel brugada SCN5A mutation leading to ST segment elevation in the inferior or the right precordial leads. J. Cardiovasc. Electrophysiol. *14*, 200–203.
41. Itoh, H., Berthet, M., Fressart, V., Denjoy, I., Maugenre, S., Klug, D., Mizusawa, Y., Makiyama, T., Hofman, N., Stallmeyer, B., et al. (2016). Asymmetry of parental origin in long QT syndrome: preferential maternal transmission of KCNQ1 variants linked to channel dysfunction. Eur. J. Hum. Genet. *24*, 1160–1166.
42. Yue, P., Li, Z., and Moult, J. (2005). Loss of protein structure stability as a major causative factor in monogenic disease. J. Mol. Biol. *353*, 459–473.
43. Stein, A., Fowler, D.M., Hartmann-Petersen, R., and Lindorff-Larsen, K. (2019). Biophysical and Mechanistic Models for Disease-Causing Protein Variants. Trends Biochem. Sci. *44*, 575–588.
44. Park, H., Bradley, P., Greisen, P., Jr., Liu, Y., Mulligan, V.K., Kim, D.E., Baker, D., and DiMaio, F. (2016). Simultaneous Optimization of Biomolecular Energy Functions on Features from Small Molecules and Macromolecules. J. Chem. Theory Comput. *12*, 6201–6212.
45. Kim, M.K., and Kang, Y.K. (1999). Positional preference of proline in alpha-helices. Protein Sci. *8*, 1492–1499.
46. Brnich, S.E., Abou Tayoun, A.N., Couch, F.J., Cutting, G.R., Greenblatt, M.S., Heinen, C.D., Kanavy, D.M., Luo, X., McNulty, S.M., Starita, L.M., et al.; Clinical Genome Resource Sequence Variant Interpretation Working Group (2019). Recommendations for application of the functional evidence PS3/BS3 criterion using the ACMG/AMP sequence variant interpretation framework. Genome Med. *12*, 3.
47. Wilde, A.A.M., and Amin, A.S. (2018). Clinical Spectrum of SCN5A Mutations: Long QT Syndrome, Brugada Syndrome, and Cardiomyopathy. JACC Clin. Electrophysiol. *4*, 569–579.
48. Milman, A., Gourraud, J.B., Andorin, A., Postema, P.G., Sacher, F., Mabo, P., Conte, G., Giustetto, C., Sarquella-Brugada, G., Hochstadt, A., et al. (2018). Gender differences in patients with Brugada syndrome and arrhythmic events: Data from a survey on arrhythmic events in 678 patients. Heart Rhythm *15*, 1457–1465.
49. Bezzina, C.R., Barc, J., Mizusawa, Y., Remme, C.A., Gourraud, J.B., Simonet, F., Verkerk, A.O., Schwartz, P.J., Crotti, L., Dagradi, F., et al. (2013). Common variants at SCN5A-SCN10A and HEY2 are associated with Brugada syndrome, a rare disease with high risk of sudden cardiac death. Nat. Genet. *45*, 1044–1049.
50. Takehara, N., Makita, N., Kawabe, J., Sato, N., Kawamura, Y., Kitabatake, A., and Kikuchi, K. (2004). A cardiac sodium channel mutation identified in Brugada syndrome associated with atrial standstill. J. Intern. Med. *255*, 137–142.
51. Probst, V., Allouis, M., Sacher, F., Pattier, S., Babuty, D., Mabo, P., Mansourati, J., Victor, J., Nguyen, J.M., Schott, J.J., et al. (2006). Progressive cardiac conduction defect is the prevailing phenotype in carriers of a Brugada syndrome SCN5A mutation. J. Cardiovasc. Electrophysiol. *17*, 270–275.

52. Remme, C.A., Wilde, A.A., and Bezzina, C.R. (2008). Cardiac sodium channel overlap syndromes: different faces of SCN5A mutations. Trends Cardiovasc. Med. *18*, 78–87.
53. Frigo, G., Rampazzo, A., Bauce, B., Pilichou, K., Beffagna, G., Danieli, G.A., Nava, A., and Martini, B. (2007). Homozygous SCN5A mutation in Brugada syndrome with monomorphic ventricular tachycardia and structural heart abnormalities. Europace *9*, 391–397.
54. Makielski, J.C., Ye, B., Valdivia, C.R., Pagel, M.D., Pu, J., Tester, D.J., and Ackerman, M.J. (2003). A ubiquitous splice variant and a common polymorphism affect heterologous expression of recombinant human SCN5A heart sodium channels. Circ. Res. *93*, 821–828.
55. Anderson, C.L., Delisle, B.P., Anson, B.D., Kilby, J.A., Will, M.L., Tester, D.J., Gong, Q., Zhou, Z., Ackerman, M.J., and January, C.T. (2006). Most LQT2 mutations reduce Kv11.1 (hERG) current by a class 2 (trafficking-deficient) mechanism. Circulation *113*, 365–373.
56. Casadio, R., Vassura, M., Tiwari, S., Fariselli, P., and Luigi Martelli, P. (2011). Correlating disease-related mutations to their effect on protein stability: a large-scale analysis of the human proteome. Hum. Mutat. *32*, 1161–1170.
57. DePristo, M.A., Weinreich, D.M., and Hartl, D.L. (2005). Missense meanderings in sequence space: a biophysical view of protein evolution. Nat. Rev. Genet. *6*, 678–687.
58. Tokuriki, N., and Tawfik, D.S. (2009). Stability effects of mutations and protein evolvability. Curr. Opin. Struct. Biol. *19*, 596–604.
59. Zhou, Y., and Bowie, J.U. (2000). Building a thermostable membrane protein. J. Biol. Chem. *275*, 6975–6979.
60. Chavali, N.V., Kryshtal, D.O., Parikh, S.S., Wang, L., Glazer, A.M., Blackwell, D.J., Kroncke, B.M., Shoemaker, M.B., and Knollmann, B.C. (2019). Patient-independent human induced pluripotent stem cell model: A new tool for rapid determination of genetic variant pathogenicity in long QT syndrome. Heart Rhythm *16*, 1686–1695.
61. Fatima, A., Kaifeng, S., Dittmann, S., Xu, G., Gupta, M.K., Linke, M., Zechner, U., Nguemo, F., Milting, H., Farr, M., et al. (2013). The disease-specific phenotype in cardiomyocytes derived from induced pluripotent stem cells of two long QT syndrome type 3 patients. PLoS ONE *8*, e83005.
62. Selga, E., Sendfeld, F., Martinez-Moreno, R., Medine, C.N., Tura-Ceide, O., Wilmut, S.I., Pérez, G.J., Scornik, F.S., Brugada, R., and Mills, N.L. (2018). Sodium channel current loss of function in induced pluripotent stem cell-derived cardiomyocytes from a Brugada syndrome patient. J. Mol. Cell. Cardiol. *114*, 10–19.
63. Heyne, H.O., Baez-Nieto, D., Iqbal, S., Palmer, D., Brunklaus, A., the Epi25 Collaborative, Johannesen, K.M., Lauxmann, S., Lemke, J.R., Moller, R.S., et al. (2019). Predicting functional effects of missense variants in the voltage-gated sodium and calcium channels. bioRxiv. https://doi.org/10.1101/671453.
64. Li, B., Mendenhall, J.L., Kroncke, B.M., Taylor, K.C., Huang, H., Smith, D.K., Vanoye, C.G., Blume, J.D., George, A.L., Jr., Sanders, C.R., and Meiler, J. (2017). Predicting the Functional Impact of KCNQ1 Variants of Unknown Significance. Circ Cardiovasc Genet *10*, 10.
65. Findlay, G.M., Daza, R.M., Martin, B., Zhang, M.D., Leith, A.P., Gasperini, M., Janizek, J.D., Huang, X., Starita, L.M., and Shendure, J. (2018). Accurate classification of BRCA1 variants with saturation genome editing. Nature *562*, 217–222.
66. Glazer, A.M., Kroncke, B.M., Matreyek, K.A., Yang, T., Wada, Y., Shields, T., Salem, J.E., Fowler, D.M., and Roden, D.M. (2020). Deep Mutational Scan of an SCN5A voltage sensor. Circ Genom Precis Med *13*, e002786.
67. Matreyek, K.A., Starita, L.M., Stephany, J.J., Martin, B., Chiasson, M.A., Gray, V.E., Kircher, M., Khechaduri, A., Dines, J.N., Hause, R.J., et al. (2018). Multiplex assessment of protein variant abundance by massively parallel sequencing. Nat. Genet. *50*, 874–882.
68. Aiba, T., Farinelli, F., Kostecki, G., Hesketh, G.G., Edwards, D., Biswas, S., Tung, L., and Tomaselli, G.F. (2014). A mutation causing Brugada syndrome identifies a mechanism for altered autonomic and oxidant regulation of cardiac sodium currents. Circ Cardiovasc Genet *7*, 249–256.
69. Casini, S., Albesa, M., Wang, Z., Portero, V., Ross-Kaschitza, D., Rougier, J.S., Marchal, G.A., Chung, W.K., Bezzina, C.R., Abriel, H., and Remme, C.A. (2019). Functional Consequences of the *SCN5A*-p.Y1977N Mutation within the PY Ubiquitylation Motif: Discrepancy between HEK293 Cells and Transgenic Mice. Int. J. Mol. Sci. *20*, 11.
70. Clatot, J., Hoshi, M., Wan, X., Liu, H., Jain, A., Shinlapawittayatorn, K., Marionneau, C., Ficker, E., Ha, T., and Deschênes, I. (2017). Voltage-gated sodium channels assemble and gate as dimers. Nat. Commun. *8*, 2077.

The American Journal of Human Genetics, Volume *107*

Supplemental Data

High-Throughput Reclassification of *SCN5A* Variants

Andrew M. Glazer, Yuko Wada, Bian Li, Ayesha Muhammad, Olivia R. Kalash, Matthew J. O'Neill, Tiffany Shields, Lynn Hall, Laura Short, Marcia A. Blair, Brett M. Kroncke, John A. Capra, and Dan M. Roden

Table of Contents

Figure S1. Diagram of cloning and cell line generation

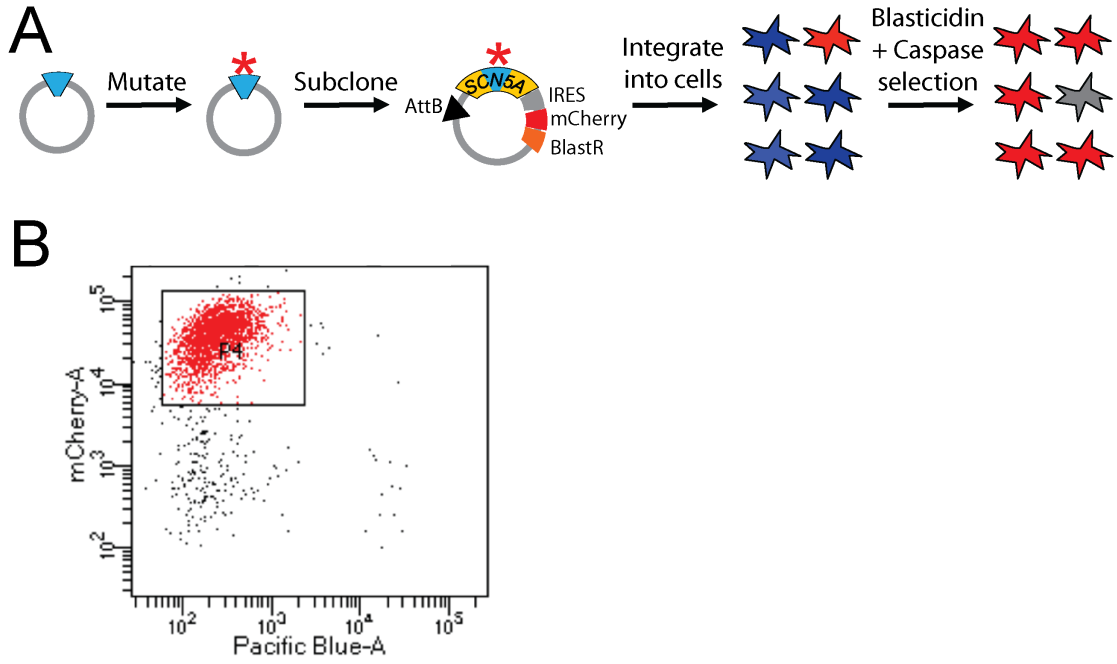

Figure S2. Voltage protocols used in this study

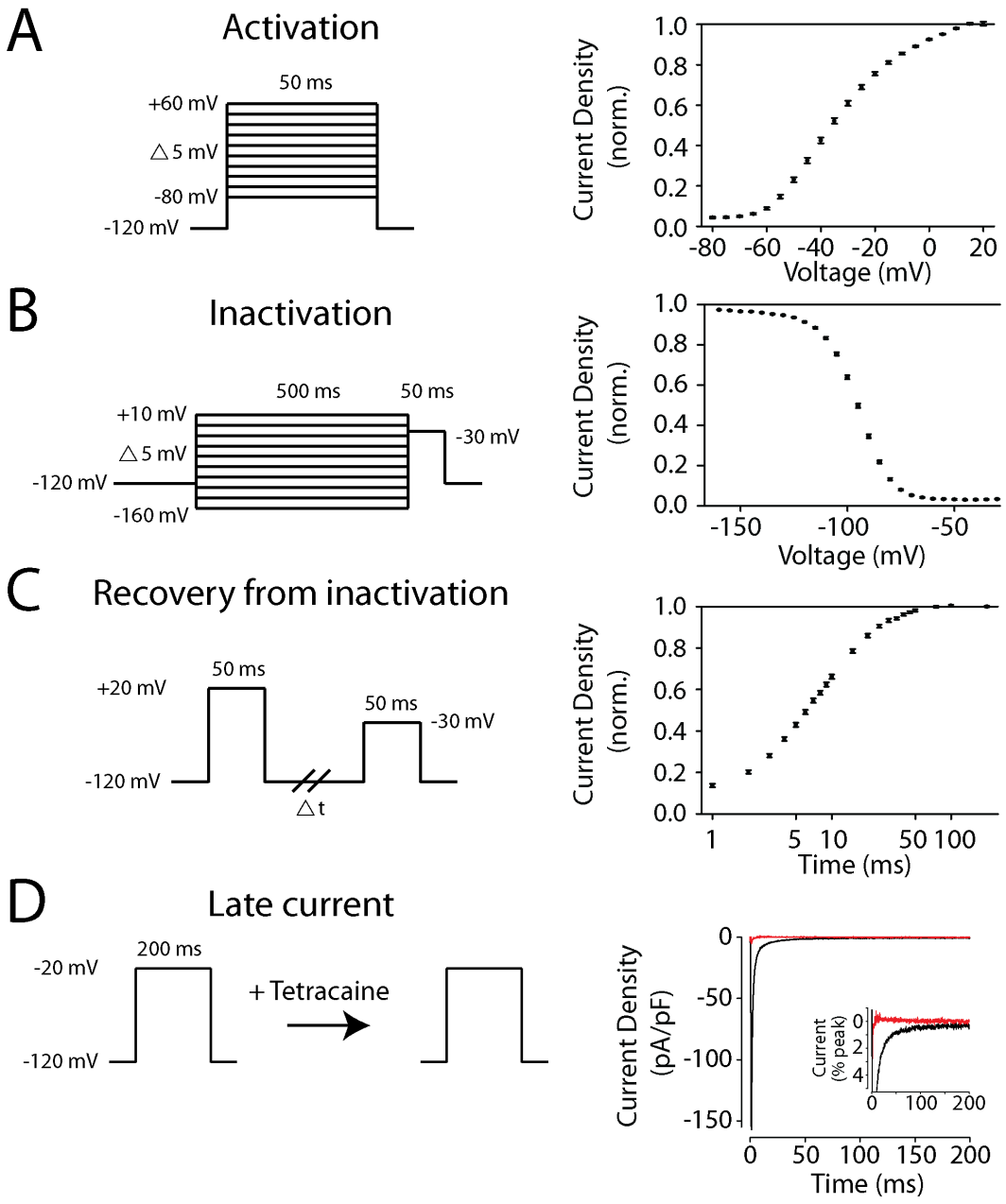

Figure S3. Example sodium current traces from included and excluded wells

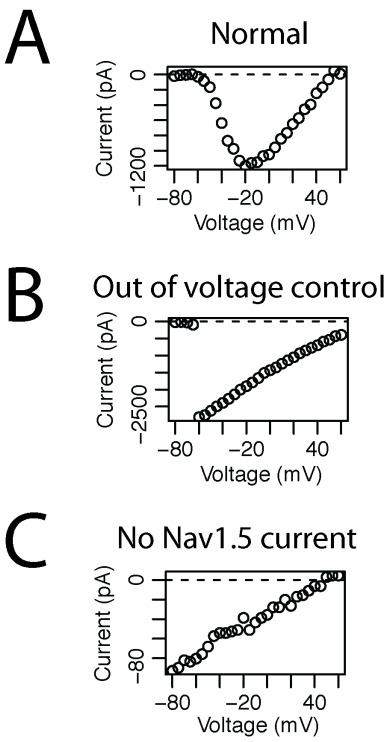

A) Example well with $Na_V1.5$ current that would be included in the analysis. B) Example well with $Na_V1.5$ current that is out of voltage control. This well would be excluded from the analysis. C) Example well with no substantial $Na_V1.5$ current. Note the difference in y-axis scale between panels.

Figure S4: Classification criteria

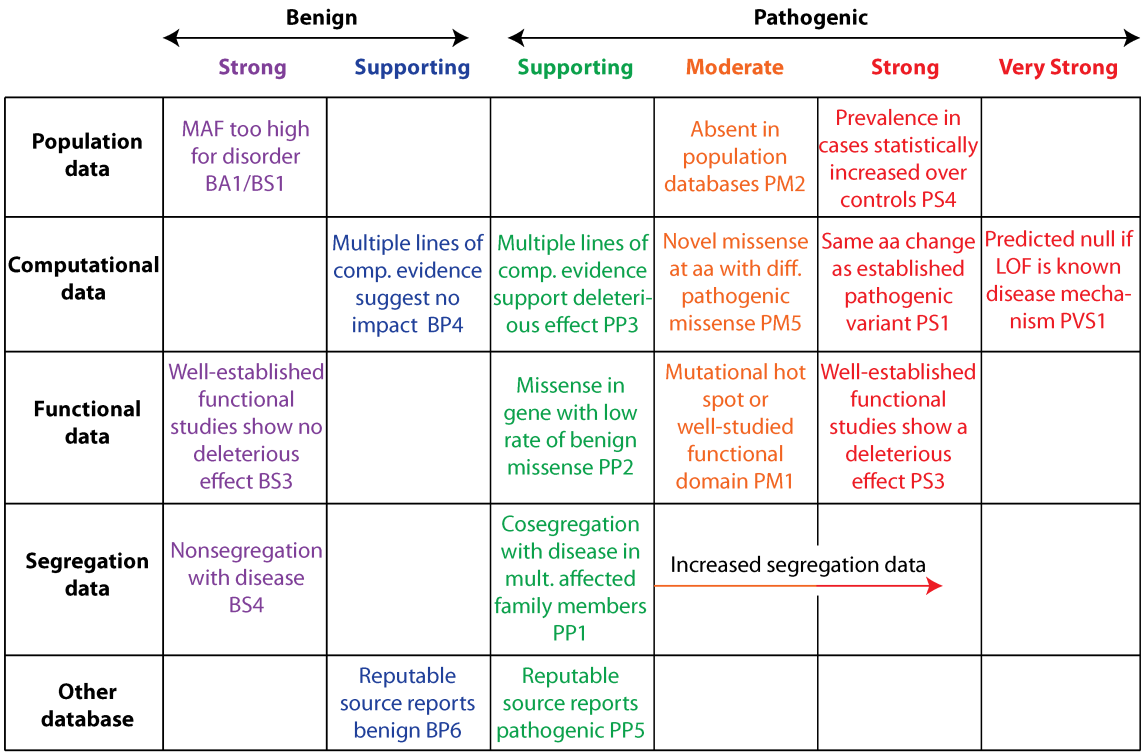

Diagram of American College of Medical Genetics and Genomics classification criteria, with a focus on criteria relevant for classification of *SCN5A* missense variants. Figure is adapted from Richards et al, 2015.[1]

Figure S5. A structural model of human $Na_V1.5$

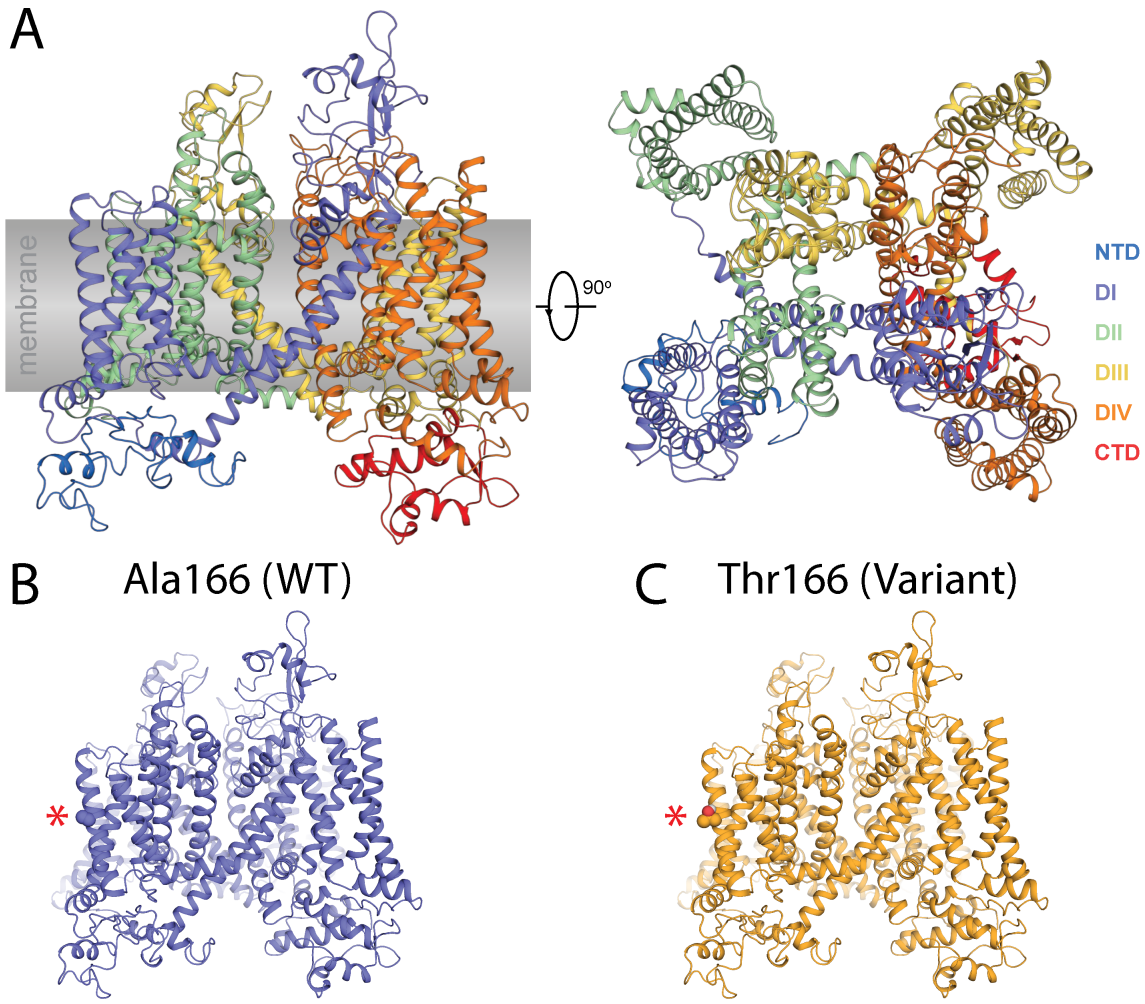

A) Wildtype $Na_V1.5$ model. The N-terminal domain (NTD), four homologous ion channel domains (DI through DIV) each consisting of six transmembrane helices, and C-terminal domain (CTD) are color-coded. B-C) A suspected benign variant, p.Ala166Thr, has a low predicted impact on protein structure and wild-type-like electrophysiological properties.

Figure S6: Voltage dependence of activation

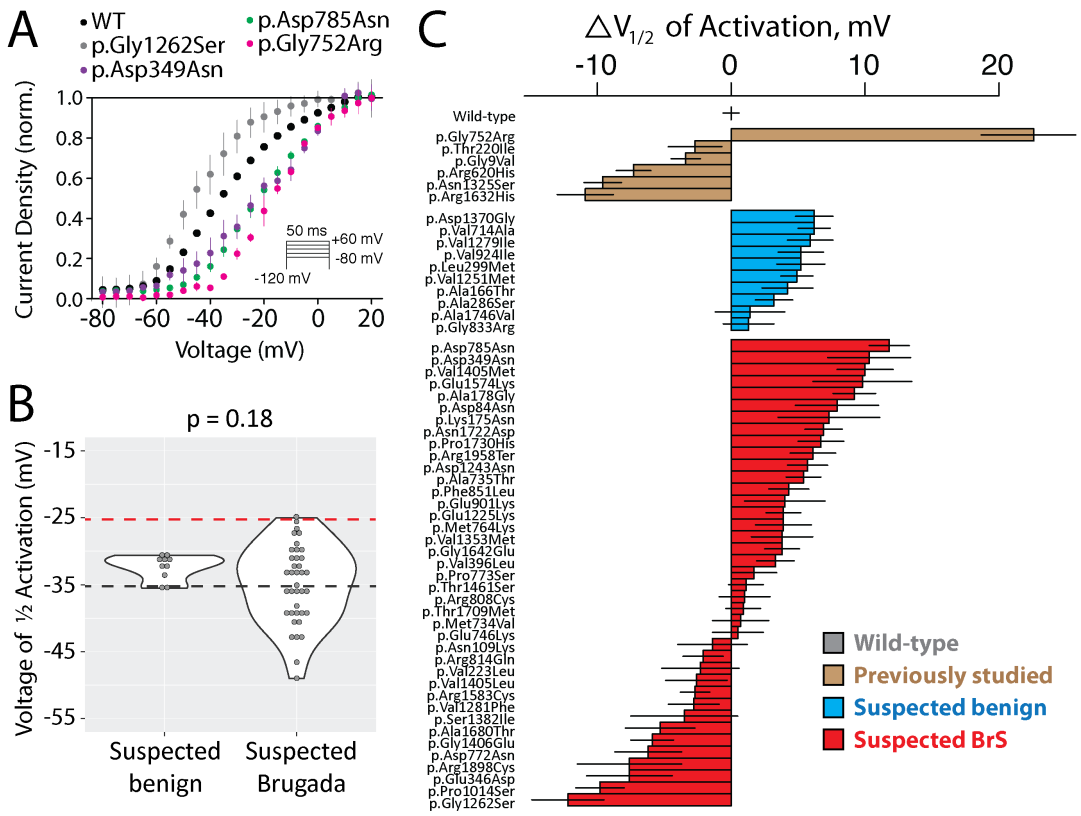

A) Normalized activation curves for wild-type, p.Asp785Asn and p.Asp349Asn (the two suspected BrS-associated variants with >10 mV rightward shifts in $V_{1/2}$ activation), p.Gly1262Ser (a suspected Brs-associated variant with a leftward shift) and p.Gly752Arg, a previously studied variant with a large rightward shift, as has previously been observed.[2] All of these variants also have a reduction in peak current (Figure 2). Error bars indicate standard error of the mean. B) Violin plot of $V_{1/2}$ activation. Black line indicates wild-type value and red line indicates a 10 mV shift in activation. Two variants, p.Asp785Asn and p.Asp349Asn, have >10 mV rightward shift in activation voltage. Panel same as Figure 2E. C) Barplot of wild-type (grey), previously studied (brown), suspected benign (blue), or suspected Brugada Syndrome-associated voltage of ½ activation. Bars indicate mean +/- standard errors. Only variants with

at least 5 qualifying cells were included, so most severe loss of function variants are not included.

Figure S7: Inactivation time

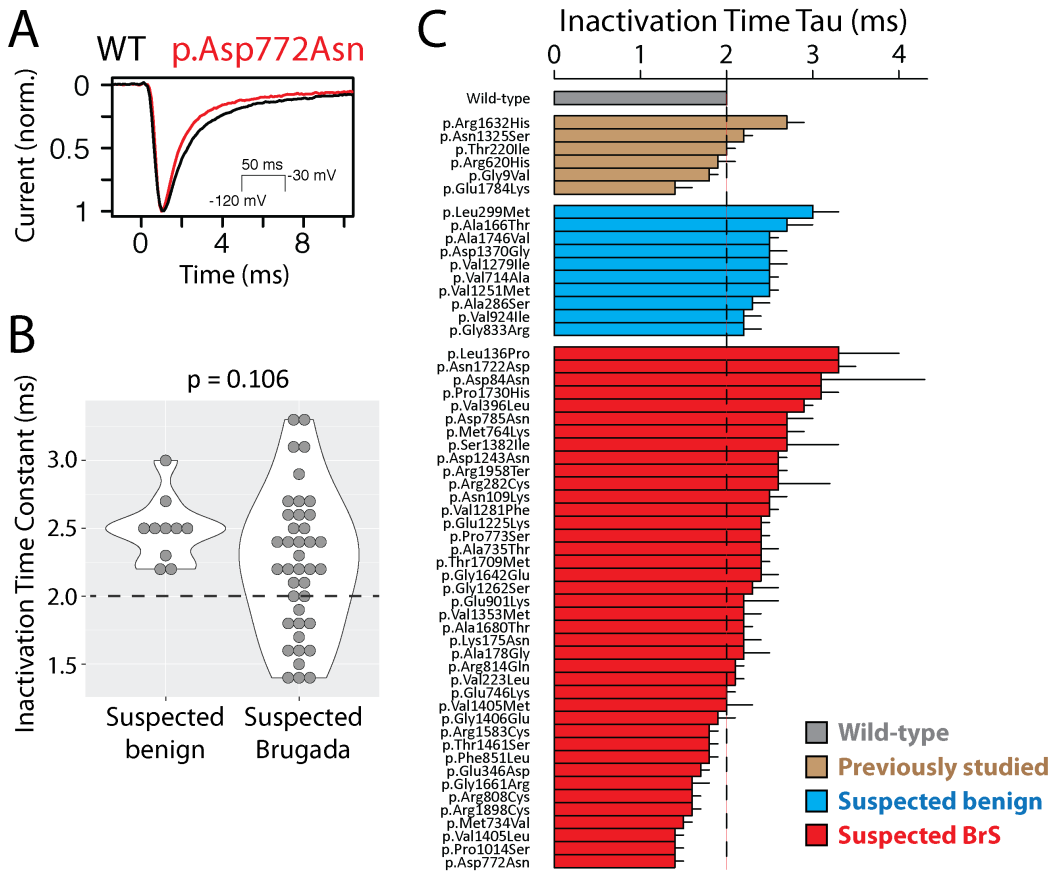

A) Inactivation time for wild-type and the suspected Brugada Syndrome-associated variant with the shortest time constant of inactivation, p.Asp772Asn. Inactivation time was measured from a 50ms pulse from -120 mV to -30 mV. Representative traces that had inactivation time constants closest to the mean values were selected. B) Violin plot of inactivation time constant. Black line indicates wild-type value. C) Barplot of wild-type (grey), previously studied (brown), suspected benign (blue), or suspected Brugada Syndrome-associated inactivation time. Bars indicate mean +/- standard errors. Only variants with at least 5 qualifying cells were included, so most severe loss of function variants are not included.

Figure S8: Voltage dependence of inactivation

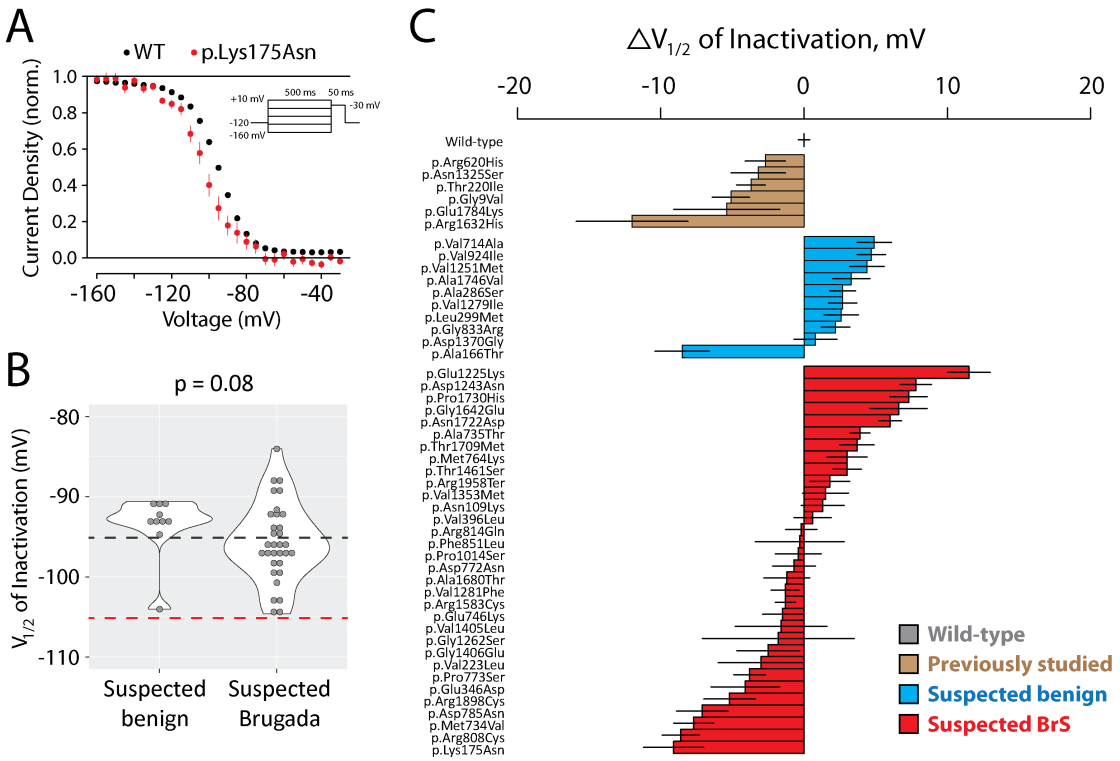

A) Normalized inactivation curves for wild-type and p.Lys175Asn, a suspected Brugada syndrome-associated variant that has the largest observed leftward shift in $V_{1/2}$ inactivation. Error bars indicate standard error of the mean. B) Violin plot of $V_{1/2}$ inactivation. Black line indicates wild-type value and red line indicates a 10 mV shift in inactivation. No previously unstudied variants had a >10 mV leftward shift in inactivation voltage. C) Barplot of wild-type (grey), previously studied (brown), suspected benign (blue), or suspected Brugada Syndrome-associated voltage of ½ inactivation. Bars indicate mean +/- standard errors. Only variants with at least 5 qualifying cells were included, so most severe loss of function variants are not included.

Figure S9: Recovery from inactivation

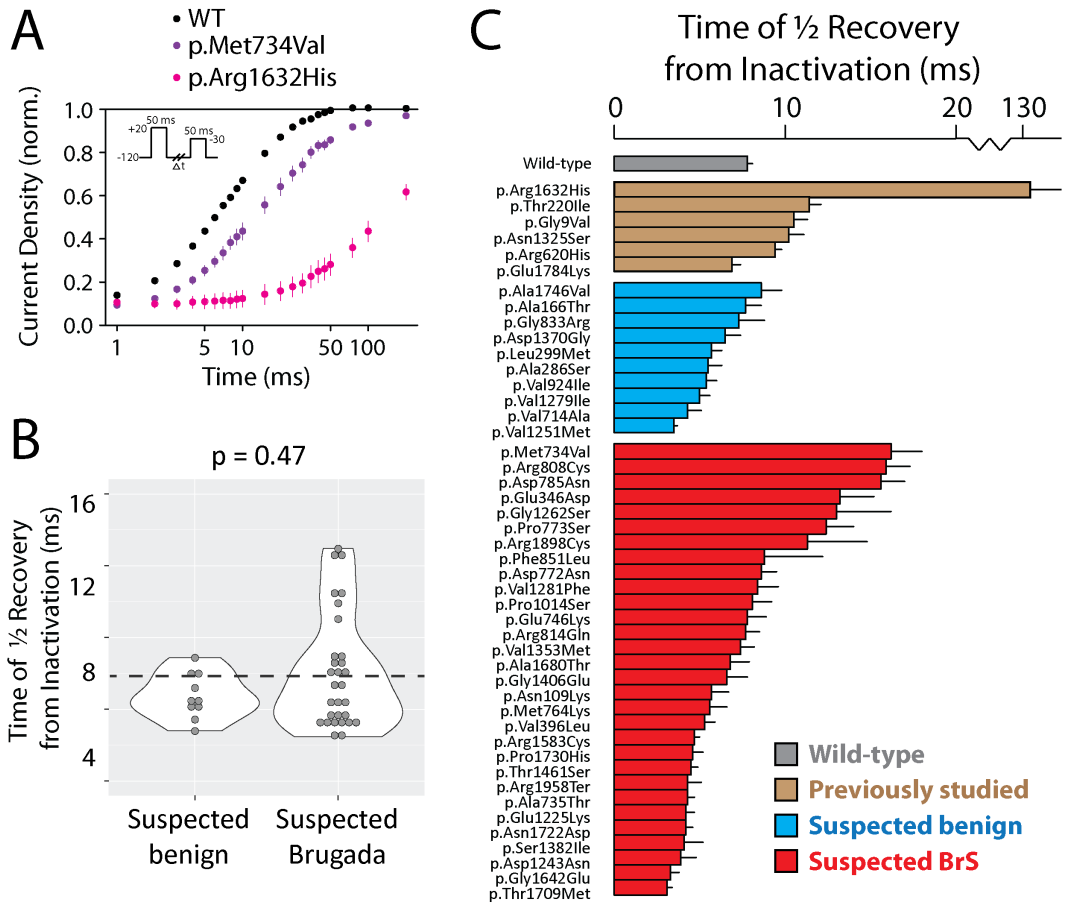

A) Normalized recovery inactivation curves for wild-type, p.Met734Val, the suspected Brugada syndrome-associated variant with the largest increase in recovery from inactivation time, and p.Arg1632His, a previously studied variant that has a very large recovery from inactivation.[3] Error bars indicate standard error of the mean. B) Violin plot of time of ½ recovery from inactivation, derived from fitting an exponential fit to the data derived from each cell. Black line indicates wild-type value. C) Barplot of wild-type (grey), previously studied (brown), suspected benign (blue), or suspected Brugada Syndrome-associated time of ½ recovery from inactivation. The X-axis has a break to accommodate the large value for p.Arg1632His. Bars

indicate mean +/- standard errors. Only variants with at least 5 qualifying cells were included, so most severe loss of function variants are not included.

Figure S10: Late current

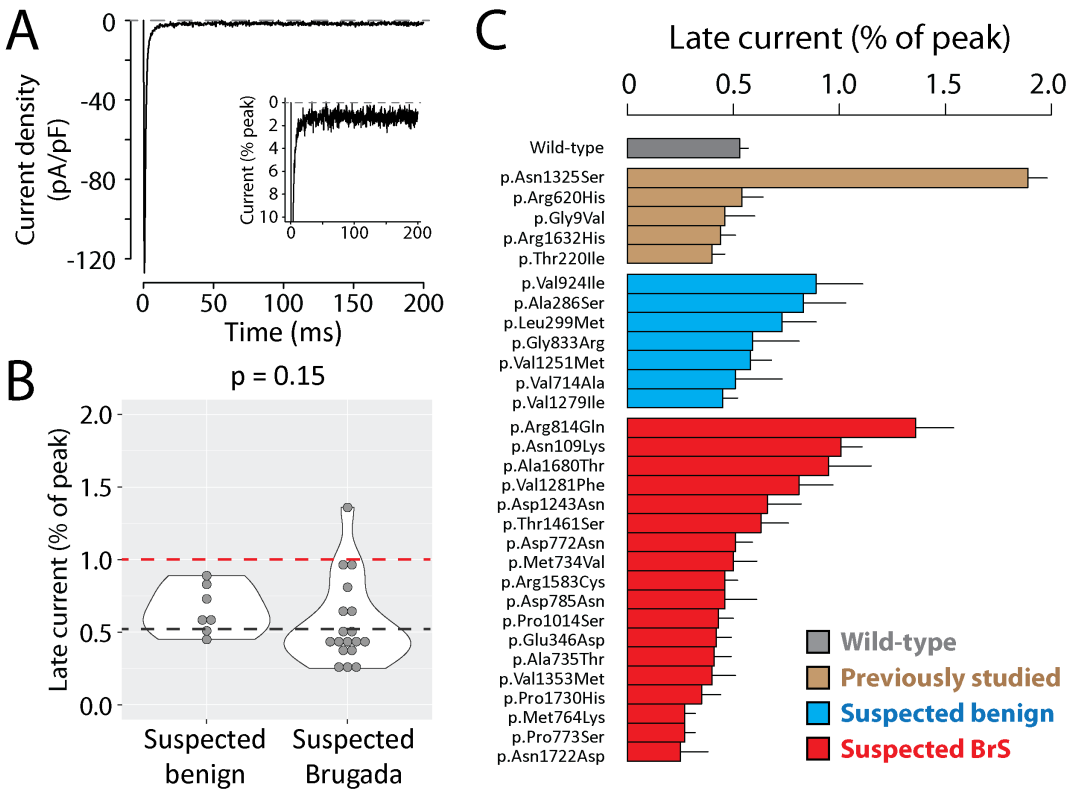

A) Tetracaine-sensitive late currents for p.Arg814Gln, the suspected Brugada syndrome-associated variant that has the largest observed increase in late current. B) Violin plot of time of late current (normalized as the percentage of peak current). Black line indicates wild-type value and red line indicates the cutoff (1%) that was considered to be deleterious. C) Barplot of wild-type (grey), previously studied (brown), suspected benign (blue), or suspected Brugada Syndrome-associated late current (normalized as the percentage of peak current). Bars indicate mean +/- standard errors. Only variants with at least 5 qualifying cells were included, so most severe loss of function variants are not included.

Figure S11. Partial rescue of loss of function variants

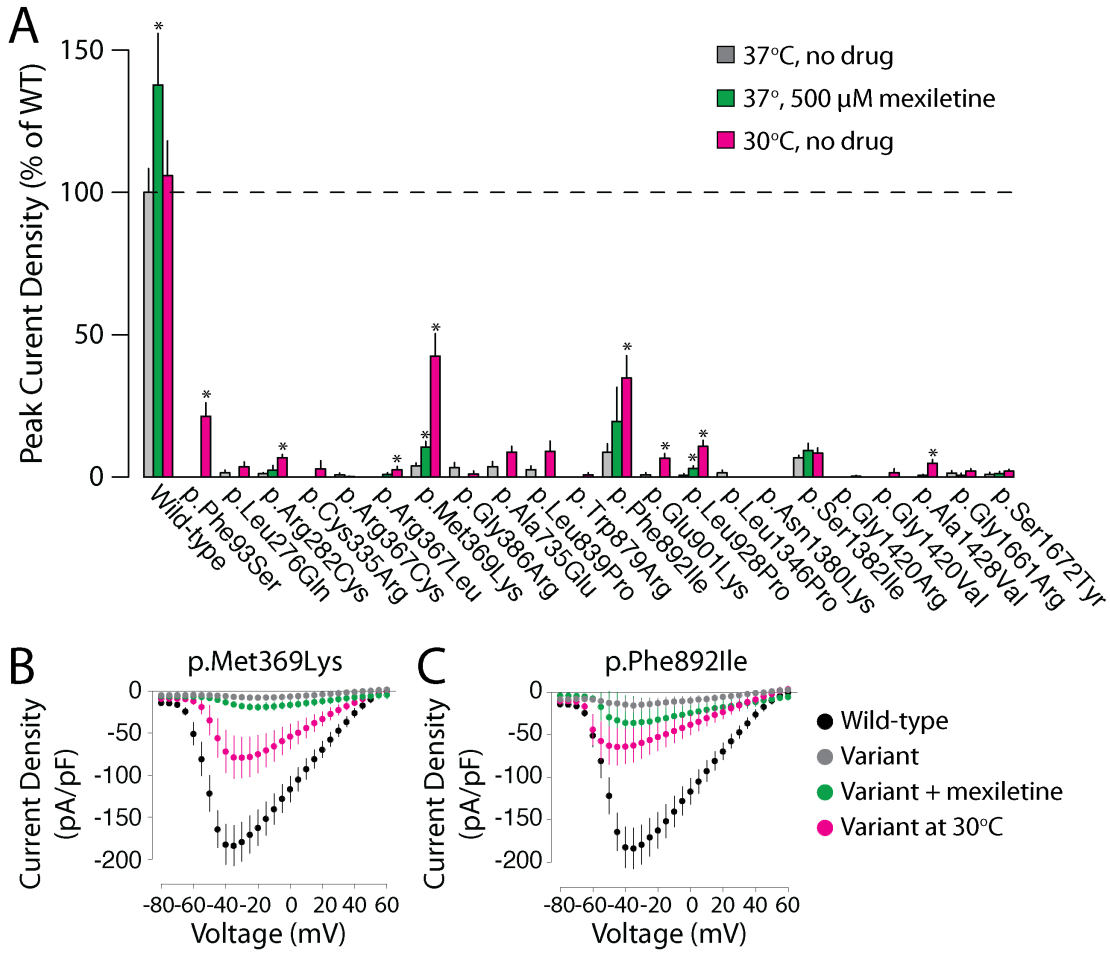

A) Peak current densities (normalized to wild-type-expressing cells from the same transfection) for the 22 variants with peak current densities <10% of wild-type. Variants were tested under usual conditions (37°, no drug, grey), with 24 hr of treatment with 500 µM mexiletine (green), or with 24 hr culture at 30° (pink). Values are mean ± standard error. *P<0.05, 2-tailed *t*-test compared with wild-type at 37° with no drug. 8/22 variants had significant increases in current at 30° and 2/22 variants had significant increases in mexiletine. B, C) Current-voltage plots for p.Met369Lys and p.Phe892Ile, the two variants with the largest response to 30°. Colors are the same as A), with black indicating wild-type at 37° with no drug.

Figure S12: Variant distance from the pore is strongly correlated with normalized peak current density

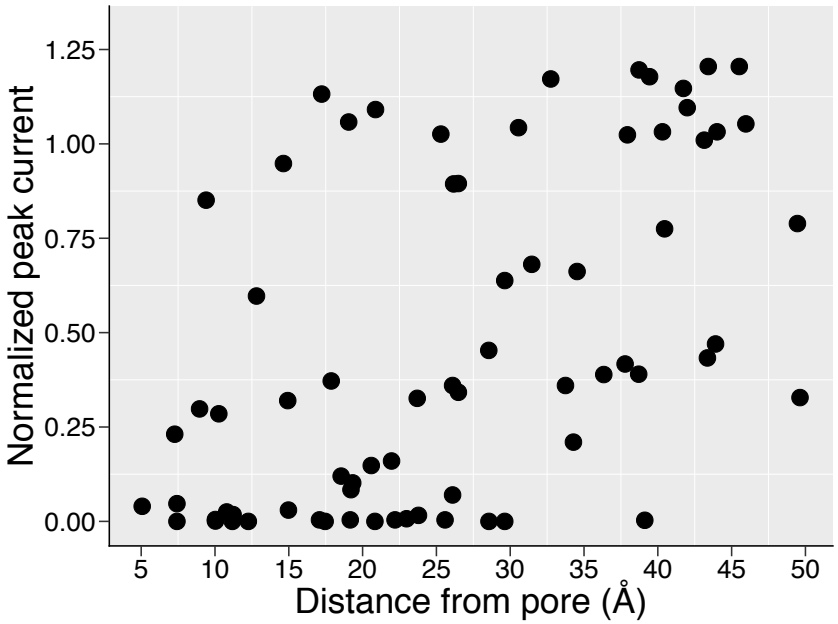

A scatter plot showing the correlation between variant distance from the pore and normalized peak currents (Pearson's $r = 0.54$, $p = 1.3\text{e} - 6$).

Figure S13. Estimated variant-induced change in thermostability is correlated with functional impact.

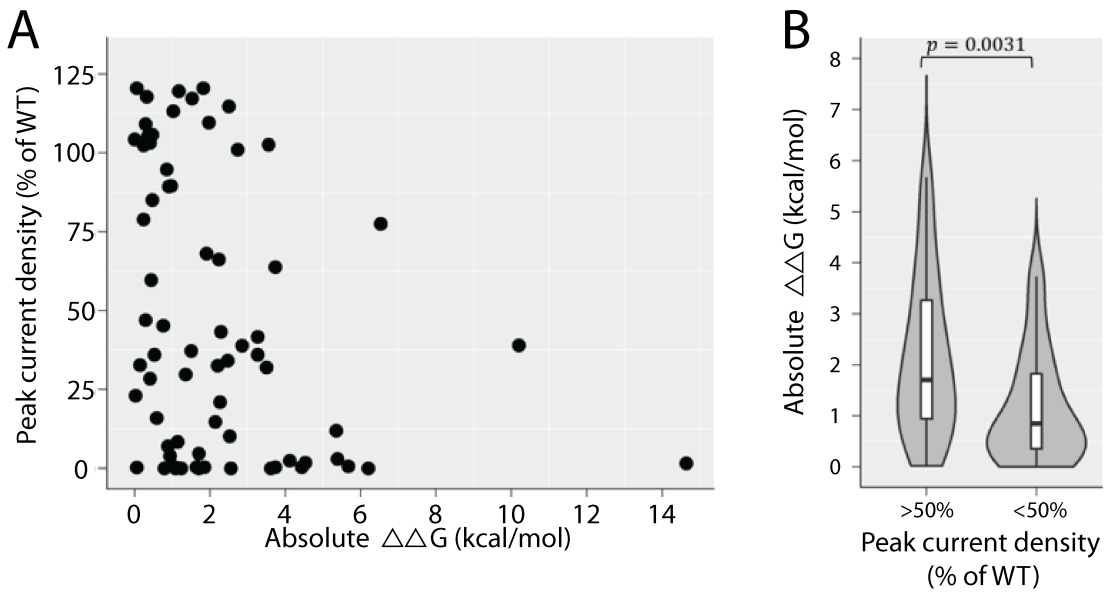

(A) A scatter plot showing the correlation between variant-induced perturbation to native thermostability (|ΔΔG|) and normalized peak currents (Pearson's $r = -0.31$, $p = 0.0092$). (B) A violin plot illustrating the distribution of absolute ΔΔG values of variants affecting SCN5A function (normalized peak current <50%, $n = 44$, median $|\Delta\Delta G| = 2.00\ kcal/mol$) and normal variants (normalized peak current >=50%, n=26 median $|\Delta\Delta G| = 0.88\ kcal/mol$, Mann-Whitney U test, $p = 0.0031$).

Figure S14. Variants may compromise function by disrupting the pore

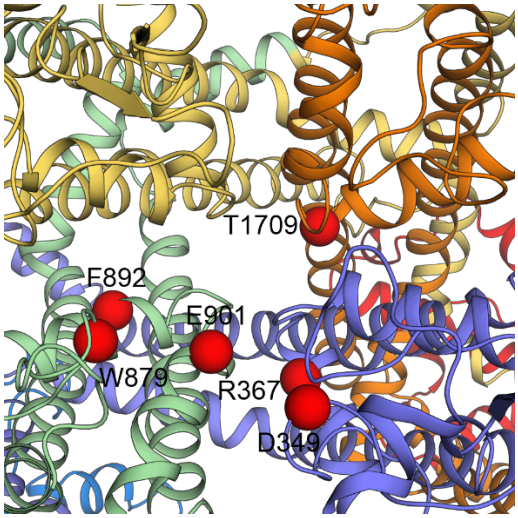

Seven pore-lining variants evaluated in this work, namely p.Asp349Asn, p.Arg367Cys, p.Arg367Leu, p.Trp879Arg, p.Phe892Ile, p.Glu901Lys, and p.Thr1709Met, cause (partial) loss of function (<50% peak current), potentially by disrupting the pore. These variants induce only minor changes in perturbations to native thermostability. The absolute ΔΔG values of these seven variants are 0.41, 1.06, 1.21, 1.09, 0.79, 0.94, 0.03 kcal/mol and the normalized peak currents are 0.29, 0.01, 0.00, 0.00, 0.00, 0.04, and 0.23, respectively. Domains are color coded as in Fig. S4. The Cα atoms of mutated residues are rendered as red spheres. p.Glu901Lys is further highlighted in Figure 5D.

Table S1. Literature and gnomAD counts, peak current density, and classifications

Class	Variant	BrS1	LQT3	Unaff.	gnomAD v2.1	Peak Curr. Density (% of WT)	ACMG Classification	
							Pre	Post
Wild-type	WT	*	*	*	*	100 (3.7)	*	*
Previously Studied	p.Gly9Val	0	1	0	0	115.6 (24.7)	VUS	VUS
	p.Arg121Trp	3	0	0	0	0.7 (0.6)	LP	LP
	p.Thr220Ile	2	0	2	197	86.7 (8.6)	VUS	VUS
	p.Thr353Ile	5	0	0	0	0.1 (0.1)	P	P
	p.Arg620His	1	0	3	7	113 (28.6)	B	B
	p.Gly752Arg	8	0	1	1	23.2 (7.1)	P	P
	p.Asn1325Ser	0	23	0	0	114.3 (22.4)	P(LQT)	P(LQT)
	p.Arg1432Gly	1	0	0	0	2.2 (1)	LP	LP
	p.Arg1632His	10	0	3	2	64.8 (11.1)	P	P
	p.Glu1784Lys	31	114	19	0	51.9 (18.8)	P(LQT +BrS)	P(LQT +BrS)
Suspected Benign	p.Ala166Thr	0	0	0	70	103.2 (21.8)	VUS	B
	p.Ala286Ser	0	0	1	79	105.8 (12.7)	LB	B
	p.Leu299Met	0	0	1	59	104.3 (16.3)	LB	B
	p.Val714Ala	0	0	0	16	101 (8.9)	VUS	B
	p.Gly833Arg	0	0	0	37	109.1 (14.8)	VUS	B
	p.Val924Ile	0	0	2	31	94.8 (12.6)	VUS	LB
	p.Val1251Met	0	0	1	59	120.5 (13.6)	VUS	B
	p.Val1279Ile	0	0	2	27	103.2 (12.7)	VUS	B
	p.Asp1370Gly	0	0	0	15	85.1 (10.6)	VUS	B
	p.Ala1746Val	0	0	0	15	89.4 (12.7)	VUS	B
Suspected Brugada Syndrome associated	p.Asp84Asn	2	0	0	0	32.8 (5)	VUS	LP
	p.Phe93Ser	2	0	0	0	0.2 (0.2)	VUS	LP
	p.Asn109Lys	3	0	0	1	119.6 (19.5)	VUS	LB
	p.Leu136Pro	2	0	0	0	39 (6.4)	VUS	LP
	p.Lys175Asn	1	0	0	0	117.8 (14.5)	VUS	VUS
	p.Ala178Gly	1	0	0	0	109.6 (19.8)	VUS	VUS
	p.Val223Leu	2	0	0	0	34.2 (6.7)	VUS	LP
	p.Leu276Gln	2	0	0	0	0.8 (0.6)	VUS	LP
	p.Arg282Cys	2	0	1	0	1.3 (0.3)	LP	P
	p.Cys335Arg	2	0	0	0	0 (0)	VUS	LP
	p.Glu346Asp	1	0	0	0	113.2 (13.9)	VUS	LB
	p.Asp349Asn	4	0	1	4	28.5 (7.6)	VUS	LP
	p.Arg367Cys	1	0	0	0	0 (0)	LP	P
	p.Arg367Leu	3	2	0	3	0.6 (0.4)	LP	P
	p.Met369Lys	3	0	0	0	3.4 (0.8)	VUS	LP
	p.Gly386Arg	2	0	0	0	1.2 (0.7)	VUS	LP
	p.Val396Leu	1	0	0	0	32 (5)	VUS	LP
	p.Met734Val	1	0	0	0	68.1 (8.7)	VUS	VUS
	p.Ala735Glu	2	0	0	0	0.9 (0.6)	VUS	LP
	p.Ala735Thr	3	0	1	0	63.8 (10.1)	VUS	VUS
	p.Glu746Lys	4	0	0	6	41.7 (10.8)	VUS	LP
	p.Met764Lys	2	0	0	0	77.5 (8.6)	VUS	VUS
	p.Asp772Asn	1	1	0	5	105.3 (10.8)	VUS	VUS
	p.Pro773Ser	1	0	0	0	120.5 (10.5)	VUS	VUS
	p.Asp785Asn	2	0	0	0	38.9 (7.2)	VUS	LP
	p.Arg808Cys	3	0	0	2	21 (5.1)	VUS	LP
	p.Arg814Gln	5	2	8	7	117.2 (11.7)	LP (BrS)	LP (LQT)

Suspected Brugada Syndrome associated	p.Leu839Pro	4	0	1	0	2.9 (2.1)	VUS	LP
	p.Phe851Leu	2	0	0	2	16 (2.3)	VUS	LP
	p.Trp879Arg	2	0	0	0	0 (0)	VUS	LP
	p.Phe892Ile	2	0	0	0	0.8 (0.6)	VUS	LP
	p.Glu901Lys	6	0	0	0	3.2 (0.5)	LP	P
	p.Asn927Ser	4	0	0	0	29.8 (5.7)	VUS	LP
	p.Leu928Pro	1	0	0	0	1.1 (0.8)	VUS	LP
	p.Pro1014Ser	2	0	0	0	121.4 (13.2)	VUS	LB
	p.Glu1225Lys	11	1	1	1	36 (5.9)	LP	P
	p.Asp1243Asn	5	0	1	41	114.7 (15.2)	VUS	B
	p.Gly1262Ser	4	0	0	8	47 (15.5)	VUS	VUS
	p.Val1281Phe	2	0	0	0	102.4 (15.5)	VUS	VUS
	p.Trp1345Cys	3	0	0	0	12 (2.2)	VUS	LP
	p.Leu1346Pro	2	0	0	0	1.6 (0.7)	VUS	LP
	p.Val1353Met	2	0	1	7	102.6 (16.5)	VUS	B
	p.Asn1380Lys	2	0	0	0	0.2 (0.2)	VUS	LP
	p.Ser1382Ile	3	0	5	0	3.5 (0.8)	VUS	LP
	p.Val1405Leu	2	0	0	0	13.9 (2.8)	VUS	LP
	p.Val1405Met	3	0	0	0	36 (6)	VUS	LP
	p.Gly1406Glu	2	0	0	0	32.6 (6.2)	LP	P
	p.Gly1420Arg	2	0	0	0	0 (0)	VUS	LP
	p.Gly1420Val	3	0	0	0	3 (1.5)	VUS	LP
	p.Ala1428Val	4	0	2	0	0.3 (0.3)	LP	P
	p.Tyr1449Cys	5	0	4	0	10.2 (3.4)	LP	P
	p.Thr1461Ser	2	0	2	0	59.7 (6.3)	VUS	VUS
	p.Glu1574Lys	4	0	0	0	43.3 (12.2)	VUS	LP
	p.Arg1583Cys	2	0	0	2	78.9 (7.2)	VUS	VUS
	p.Gly1642Glu	1	0	0	0	14.8 (2.5)	VUS	LP
	p.Gly1661Arg	7	0	0	0	5.4 (1.5)	LP	P
	p.Ser1672Tyr	3	0	0	0	0.9 (0.5)	VUS	LP
	p.Ala1680Thr	4	1	0	13	89.5 (14.6)	VUS	B
	p.Thr1709Met	2	1	0	1	23.1 (3.2)	VUS	LP
	p.Asn1722Asp	3	0	5	0	37.2 (3.8)	VUS	LP
	p.Pro1730His	2	0	3	0	45.3 (5.1)	VUS	LP
	p.Arg1898Cys	2	0	1	10	28.4 (8.6)	VUS	LP
	p.Arg1958Ter	0	2	0	13	59.3 (8.3)	VUS	VUS

Peak current density is normalized to WT and presented as mean (standard error).

VUS=Variant of Uncertain Significance, P=Pathogenic, LP=Likely Pathogenic, B=Benign, LB=Likely Benign. Susp. BrS = Suspected BrS, Susp. Benign = Suspected Benign, Unaff.=Unaffected, Peak curr. Density=Peak Current Density. Counts of individuals with or without disease are from a literature curation of *SCN5A* variants.[4,5] Variant classifications are for Brugada Syndrome unless otherwise indicated.

Table S2. Zone boundaries and restriction enzymes

Zone	Size (bp)	Location (bp)	Restriction enzymes
1	727	1-727	AgeI, BssHII
2	835	722-1557	BssHII, SpeI
3	683	1552-2235	SpeI, EcoRI
4	757	2230-2987	EcoRI, NheI
5	829	2982-3811	NheI, NsiI
6	790	3806-4596	NsiI, AatII
7	769	4591-5360	AatII, AflII
8	704	5355-6059	AflII, NdeI

Zone locations are slightly overlapping because each restriction enzyme site is present in two adjacent zone plasmids. Coordinates refer to the canonical numbering scheme with Gln1077 included (ENST00000333535), although the wild-type plasmid used in this study had Gln1077 deleted (ENST00000443581).

Table S3. Primers used in this study

Variant	Zone	Name	Sequence
p.Gly9Val	1	ag654	CCTATTACCTCGGGTCACCAGCAGCTTCC
p.Asp84Asn	1	ag737	CCCTGGAGGACCTGAACCCCTTCTATAGC
p.Phe93Ser	1	ag738	CTATAGCACCCAAAAGACTTCCATCGTACTGAATAAAGGCA
p.Asn109Lys	1	ag739	TTCCGGTTCAGTGCCACCAAAGCCTTGTATGTC
p.Arg121Trp	1	ag655	CTTCCACCCCATCTGGAGAGCGGCTGT
p.Leu136Pro	1	ag740	CTCGCTCTTCAACATGCCCATCATGTGCACCATCC
p.Ala166Thr	1	ag656	TCGAGTACACCTTCACCACCATTTACACCTTTGAG
p.Lys175Asn	1	ag775	TGAGTCTCTGGTCAACATTCTGGCTCGAGGC
p.Ala178Gly	1	ag776	GGTCAAGATTCTGGGTCGAGGCTTCTGCC
p.Thr220Ile	1	ag728	CTCAGCCTTACGCATCTTCCGAGTCCTCC
p.Val223Leu	1	ag741	CCTTACGCACCTTCCGACTCCTCCGGG
p.Leu276Gln	2	ag742	CTCTTCATGGGCAACCAAAGGCACAAGTGCGTG
p.Arg282Cys	2	ag729	GGCACAAGTGCGTGTGCAACTTCACAGCG
p.Ala286Ser	2	ag660	GTGCGTGCGCAACTTCACATCGCTCAACGG
p.Leu299Met	2	ag661	GGAGGCCGACGGCATGGTCTGGGAATC
p.Cys335Arg	2	ag785	GACGCTGGGACACGTCCGGAGGGCT
p.Glu346Asp	2	ag777	TAAAGGCAGGCGACAACCCCGACCACG
p.Asp349Asn	2	ag786	AGGCGAGAACCCCAACCACGGCTACAC
p.Thr353Ile	2	ag664	CCGACCACGGCTACATCAGCTTCGATTCCTT
p.Arg367Cys	2	ag778	TTTCTTGCACTCTTCCTCCTGATGACGCAGGAC
p.Arg367Leu	2	ag665	CTTTCTTGCACTCTTCTGCCTGATGACGCAGGA
p.Met369Lys	2	ag743	CTCTTCCGCCTGAAGACGCAGGACTGC
p.Gly386Arg	2	ag745	AGACCCTCAGGTCCGCAAGGAAGATCTACATG
p.Val396Leu	2	ag779	CATGATCTTCTTCATGCTTCTCATCTTCCTGGGGTC
p.Arg620His	3	ag128	AAGCCACCTCCTCCACCCTGTGATGCTAG
p.Val714Ala	3	ag691	GGAGTGAAGTTGGTGGCCATGGACCCGTTTACT
p.Met734Val	3	ag780	CTCAACACACTCTTCGTGGCGCTGGAGCACT
p.Ala735Glu	3	ag746	CAACACACTCTTCATGGAGCTGGAGCACTACAACA
p.Ala735Thr	3	ag747	TCAACACACTCTTCATGACGCTGGAGCACTACAAC
p.Glu746Lys	4	ag669	GCGGCCGCGAATTCAAGGAGATGCTGCA
p.Gly752Arg	4	ag145	GGAGATGCTGCAGGTCAGAAACCTGGTCTTCAC
p.Met764Lys	4	ag790	GGATTTTCACAGCAGAGAAGACCTTCAAGATCATTGC
p.Asp772Asn	4	ag670	TCAAGATCATTGCCCTCAACCCCTACTACTACTTC
p.Pro773Ser	4	ag781	AGATCATTGCCCTCGACTCCTACTACTACTTCCAA
p.Asp785Asn	4	ag748	AGGGCTGGAACATCTTCAACAGCATCATCGTCATC
p.Arg808Cys	4	ag672	CTTGTCGGTGCTGTGCTCCTTCCGCCT
p.Arg814Gln	4	ag674	CTTCCGCCTGCTGCAGGTCTTCAAGCTGG
p.Gly833Arg	4	ag675	ACTCATCAAGATCATCAGGAACTCAGTGGGGGC
p.Leu839Pro	4	ag749	CAGTGGGGGCACCGGGGAACCTGAC
p.Phe851Leu	4	ag799	TGCTTGCCATCATCGTGCTCATCTTTGCTGTGGTG
p.Trp879Arg	4	ag798	CCTGCTGCCTCGCAGGCACATGATGGA
p.Phe892Ile	4	ag750	GCCTTCCTCATCATCATCCGCATCCTCTGTG
p.Glu901Lys	4	ag678	CTGTGGAGAGTGGATCAAGACCATGTGGGACTG
p.Val924Ile	4	ag680	TGGTCTTCTTGCTTGTTATGATCATTGGCAACCTTGTGGTC
p.Asn927Ser	4	ag751	CTTGTTATGGTCATTGGCAGCCTTGTGGTCCTGAAT
p.Leu928Pro	4	ag782	TATGGTCATTGGCAACCCTGTGGTCCTGAATCTCT
p.Pro1014Ser	5	ag792	CCCCGCCACCCTCAGAGACGGAG
p.Glu1225Lys	5	ag687	GGAGCGCTGGCCTTCAAGGACATCTACCTAG
p.Asp1243Asn	5	ag688	GGTTCTGCTTGAGTATGCCAACAAGATGTTCACATATGT
p.Val1251Met	5	ag689	TGTTCACATATGTCTTCATGCTGGAGATGCTGCTC
p.Gly1262Ser	5	ag690	TCAAGTGGGTGGCCTACAGCTTCAAGAAGTACTTC

p.Val1279Ile	6	ag704	GCTCGACTTCCTCATCATAGATGTCTCTCTGGT
p.Val1281Phe	6	ag752	CTTCCTCATCGTAGACTTCTCTCTGGTCAGCCT
p.Asn1325Ser	6	ag132	GGCATGAGGGTGGTGGTCAGTGCCCTGGTG
p.Trp1345Cys	6	ag753	GTCTGCCTCATCTTCTGCCTCATCTTCAGCATCAT
p.Leu1346Pro	6	ag754	CTGCCTCATCTTCTGGCCCATCTTCAGCATCATGG
p.Val1353Met	6	ag697	CTTCAGCATCATGGGCATGAACCTCTTTGCGGG
p.Asp1370Gly	6	ag698	CAACCAGACAGAGGGAGGCTTGCCTTTGAACTACA
p.Asn1380Lys	6	ag755	TTTGAACTACACCATCGTGAACAAAAAGAGCCAGTGTG
p.Ser1382Ile	6	ag795	CTACACCATCGTGAACAACAAGATCCAGTGTGAGTC
p.Val1405Leu	6	ag756	AGTCAACTTTGACAACCTGGGGGCCGGGTA
p.Val1405Met	6	ag757	AAAGTCAACTTTGACAACATGGGGGCCGGGTAC
p.Gly1406Glu	6	ag758	CTTTGACAACGTGGAGGCCGGGTACCTGG
p.Gly1420Arg	6	ag759	GTCCATCCAGCGTTTAAATGTTGCCACCTGCAG
p.Gly1420Val	6	ag760	GCAGGTGGCAACATTTAAAGTCTGGATGGACATTATGTATG
p.Ala1428Val	6	ag761	GGACATTATGTATGCAGTTGTGGACTCCAGGGGG
p.Arg1432Gly	6	ag783	CAGCTGTGGACTCCGGGGGGTATGAAGAG
p.Tyr1449Cys	6	ag762	ACCTCTACATGTACATCTGTTTTGTCATTTTCATCAT
p.Thr1461Ser	6	ag796	CATCTTTGGGTCTTTCTTCTCCCTGAACCTCTTTATTGG
p.Glu1574Lys	7	ag764	TGGCCATCTTCACAGGCAAGTGTATTGTCAAGCTG
p.Arg1583Cys	7	ag794	AGCTGGCTGCCCTGTGCCACTACTACTTC
p.Arg1632His	7	ag642	GGCCCGAATAGGCCACATCCTCAGACTGA
p.Gly1642Glu	7	ag784	GAGGGGCCAAGGAGATCCGCACGCT
p.Gly1661Arg	7	ag645	GCCCTCTTCAACATCAGGCTGCTGCTCTTCC
p.Ser1672Tyr	7	ag766	CGTCATGTTCATCTACTACATCTTTGGCATGGCCA
p.Ala1680Thr	7	ag646	TTGGCATGGCCAACTTCACTTATGTCAAGTGGGAG
p.Thr1709Met	7	ag797	TTCCAGATCACCATGTCGGCCGGCTGG
p.Asn1722Asp	7	ag791	AGCCCCATCCTCGACACTGGGCCGC
p.Pro1730His	7	ag793	CCCTACTGCGACCACACTCTGCCCAAC
p.Ala1746Val	7	ag650	CGGGAGCCCAGTCGTGGGCATCC
p.Glu1784Lys	7	ag653	GGAGGAGAGCACCAAGCCCTTAAGGCG
p.Arg1898Cys	8	ag700	CCACCACACTCCGGTGCAAGCACGAAGAG
p.Arg1958Ter	8	ag734	GTGAGAACTTCTCCTGACCCCTTGGCCCA

Table S4. Reasons for cell exclusion

Parameter	Candidate cells	Inclusion criteria	Cells meeting inclusion	Good fitting best fit curve	Post-outlier removal (final)
$V_{1/2}$ activation	2010	100-2000 pA	1645	1256	1250
$V_{1/2}$ inactivation	2010	100-2000 pA	1645	1188	1150
Inactivation time	2010	100-2000 pA	1645	1440	1413
Recovery from inactivation	2010	100-2000 pA	1645	1005	1005
Late current	2010	500-2000 pA, <10% change in seal resistance/capacitance	577	577	566

Table S5. ACMG criteria used for variant classification

Class	Variant	Criteria	PS3/BS3	ACMG (Pre)	ACMG (Post)
Suspected Benign	p.Ala166Thr	PP2 BS1	BS3	VUS	B
	p.Ala286Ser	PP2 BS1 BP4	BS3	LB	B
	p.Leu299Met	PP2 BS1 BP4	BS3	LB	B
	p.Val714Ala	PP2 BS1	BS3	VUS	B
	p.Gly833Arg	PP2 PP3 BS1	BS3	VUS	B
	p.Val924Ile	PM2 PP2 BP4	BS3	VUS	LB
	p.Val1251Met	PP2 BS1	BS3	VUS	B
	p.Val1279Ile	PP2 BS1	BS3	VUS	B
	p.Asp1370Gly	PP2 BS1	BS3	VUS	B
	p.Ala1746Val	PP2 BS1	BS3	VUS	B
Suspected Brugada-associated	p.Asp84Asn	PM2 PP2 PP3	PS3	VUS	LP
	p.Phe93Ser	PM2 PP2 PP3	PS3	VUS	LP
	p.Asn109Lys	PM2 PP2 BP4	BS3	VUS	LB
	p.Leu136Pro	PM2 PP2	PS3	VUS	LP
	p.Lys175Asn	PM2 PP2 PP3	BS3	VUS	VUS
	p.Ala178Gly	PM2 PP2 PP3	BS3	VUS	VUS
	p.Val223Leu	PM2 PP2 PP3	PS3	VUS	LP
	p.Leu276Gln	PM2 PP2 PP3	PS3	VUS	LP
	p.Arg282Cys	PM2 PM5 PP2 PP3 PP5	PS3	LP	P
	p.Cys335Arg	PM2 PP2 PP3	PS3	VUS	LP
	p.Glu346Asp	PM2 PP2 BP4	BS3	VUS	LB
	p.Asp349Asn	PM2 PP2	PS3	VUS	LP
	p.Arg367Cys	PM2 PM5 PP2 PP3	PS3	LP	P
	p.Arg367Leu	PM2 PM5 PP2 PP3 PP5	PS3	LP	P
	p.Met369Lys	PM2 PP2 PP3	PS3	VUS	LP
	p.Gly386Arg	PM2 PP2 PP3	PS3	VUS	LP
	p.Val396Leu	PM2 PP2 PP3	PS3	VUS	LP
	p.Met734Val	PM2 PP2	*	VUS	VUS
	p.Ala735Glu	PM2 PM5 PP2	PS3	VUS	LP
	p.Ala735Thr	PM2 PM5 PP2	*	VUS	VUS
	p.Glu746Lys	PM2 PP2 BP4	PS3	VUS	LP
	p.Met764Lys	PM2 PP2	BS3	VUS	VUS
	p.Asp772Asn	PM2 PP2	BS3	VUS	VUS
	p.Pro773Ser	PM2 PP2	BS3	VUS	VUS
	p.Asp785Asn	PM2 PP2 PP3	PS3	VUS	LP
	p.Arg808Cys	PM2 PP2 PP3	PS3	VUS	LP
	p.Arg814Gln	PS4 PP2 PP3 BS1	PS3 (LQT)	LP (BrS)	LP (LQT)
	p.Leu839Pro	PM2 PP2 PP3	PS3	VUS	LP
	p.Phe851Leu	PM2 PP2 PP3	PS3	VUS	LP
	p.Trp879Arg	PM2 PP2 PP3	PS3	VUS	LP
	p.Phe892Ile	PM2 PP2	PS3	VUS	LP
	p.Glu901Lys	PS4 PM2 PP2 PP3	PS3	LP	P
	p.Asn927Ser	PM2 PP2	PS3	VUS	LP
	p.Leu928Pro	PM2 PP2	PS3	VUS	LP
	p.Pro1014Ser	PM2 PP2 BP4	BS3	VUS	LB

Suspected Brugada-associated	p.Glu1225Lys	PS4 PM2 PP2 PP3	PS3	LP	P
	p.Asp1243Asn	PP2 PP3 BS1	BS3	VUS	B
	p.Gly1262Ser	PP2 PP3 BS1	*	VUS	VUS
	p.Val1281Phe	PM2 PP2 PP3	BS3	VUS	VUS
	p.Trp1345Cys	PM2 PP2 PP3	PS3	VUS	LP
	p.Leu1346Pro	PM2 PP2 PP3	PS3	VUS	LP
	p.Val1353Met	PP2 PP3 BS1	BS3	VUS	B
	p.Asn1380Lys	PM2 PP2 PP3	PS3	VUS	LP
	p.Ser1382Ile	PM2 PP2 PP3	PS3	VUS	LP
	p.Val1405Leu	PM2 PP2 PP3	PS3	VUS	LP
	p.Val1405Met	PM2 PP2 PP3	PS3	VUS	LP
	p.Gly1406Glu	PM2 PM5 PP2 PP3	PS3	LP	P
	p.Gly1420Arg	PM2 PP2 PP3	PS3	VUS	LP
	p.Gly1420Val	PM2 PP2 PP3	PS3	VUS	LP
	p.Ala1428Val	PM2 PM5 PP2 PP3	PS3	LP	P
	p.Tyr1449Cys	PS4 PM2 PP2 PP3 PP5	PS3	LP	P
	p.Thr1461Ser	PM2 PP2	*	VUS	VUS
	p.Glu1574Lys	PM2 PP2 PP3	PS3	VUS	LP
	p.Arg1583Cys	PM2 PP2 PP3	BS3	VUS	VUS
	p.Gly1642Glu	PM2 PP2 PP3	PS3	VUS	LP
	p.Gly1661Arg	PS4 PM2 PP2 PP3	PS3	LP	P
	p.Ser1672Tyr	PM2 PP2 PP3	PS3	VUS	LP
	p.Ala1680Thr	PP2 PP3 BS1	BS3	VUS	B
	p.Thr1709Met	PM2 PP2 PP3	PS3	VUS	LP
	p.Asn1722Asp	PM2 PP2 PP3	PS3	VUS	LP
	p.Pro1730His	PM2 PP2 PP3	PS3	VUS	LP
	p.Arg1898Cys	PP2 PP3 BS1	PS3	VUS	LP
	p.Arg1958Ter	PM4	*	VUS	VUS

American College of Medical Genetics (ACMG) criteria were adapted from Richards et al[1] as described in the methods. ACMG (Pre) and ACMG (Post) indicate the ACMG classification before and after patch clamp data from this study are included, respectively.

Table S6. Summary of the Rosetta energy functions used for $\Delta\Delta G$ calculation

Energy term	Weight	Description
fa_atr	0.18	Lennard-Jones attractive between atoms in different residues
fa_dun	0.07	Internal energy of sidechain rotamers as derived from Dunbrack's statistics
fa_mbenv	0.17	Statistics-based depth-dependent membrane environment potential
fa_mpsolv	0.23	Statistics-based depth- and burial-dependent solvation potential
fa_pair	0.57	Statistics-based amino-acid pair potential, favors salt bridges
fa_rep	0.08	Lennard-Jones repulsive between atoms in different residues
hbond_bb_sc	0.45	Sidechain-backbone hydrogen bond energy
hbond_sc	0.43	Sidechain-sidechain hydrogen bond energy
omega	0.09	Omega dihedral in the backbone. A harmonic constraint on planarity with standard deviation of ~6 degrees

Table S7. All measured parameters for each variant

Variant	n	Peak density	V1/2 Activation	Inact. time	V1/2 Inactivation	Rec. from Inactivation	Late (% peak)
WT	471	100 (3.7)	-36.8 (0.6)	2 (0)	-95.5 (0.4)	7.8 (0.3)	0.53 (0.04)
p.Gly9Val	19	115.6 (24.7)	-40.2 (1.1)	1.8 (0.1)	-100.6 (1.3)	10.5 (0.8)	0.46 (0.14)
p.Arg121Trp	17	0.7 (0.6)	*	*	*	*	*
p.Thr220Ile	28	86.7 (8.6)	-39.5 (2)	2 (0.1)	-99.2 (1)	11.4 (0.7)	0.4 (0.06)
p.Thr353Ile	19	0.1 (0.1)	*	*	*	*	*
p.Arg620His	17	113 (28.6)	-44.1 (1.3)	1.9 (0.2)	-98.2 (1.4)	9.4 (0.4)	0.54 (0.1)
p.Gly752Arg	14	23.2 (7.1)	-14.2 (2.4)	*	*	*	*
p.Asn1325Ser	16	114.3 (22.4)	-46.4 (1.4)	2.2 (0.1)	-98.7 (1.9)	10.2 (0.9)	1.89 (0.09)
p.Arg1432Gly	16	2.2 (1)	*	*	*	*	*
p.Arg1632His	31	64.8 (11.1)	-47.7 (2.1)	2.7 (0.2)	-107.5 (3.9)	133.9 (13)	0.44 (0.07)
p.Glu1784Lys	12	51.9 (18.8)	*	1.4 (0.2)	-100.9 (3.7)	6.9 (0.5)	*
p.Ala166Thr	37	103.2 (21.8)	-32.6 (1.9)	2.7 (0.3)	-104 (1.9)	7.7 (0.9)	*
p.Ala286Ser	36	105.8 (12.7)	-33.6 (1.4)	2.3 (0.2)	-92.8 (0.9)	5.5 (0.8)	0.83 (0.2)
p.Leu299Met	30	104.3 (16.3)	-31.6 (1.8)	3 (0.3)	-92.9 (1.2)	5.7 (0.6)	0.73 (0.16)
p.Val714Ala	41	101 (8.9)	-30.6 (1.2)	2.5 (0.1)	-90.6 (1.2)	4.3 (0.8)	0.51 (0.22)
p.Gly833Arg	26	109.1 (14.8)	-35.5 (1.9)	2.2 (0.2)	-93.3 (1)	7.3 (1.5)	0.59 (0.22)
p.Val924Ile	33	94.8 (12.6)	-31.6 (1.7)	2.2 (0.2)	-90.8 (1)	5.4 (0.6)	0.89 (0.22)
p.Val1251Met	33	120.5 (13.6)	-31.9 (1.2)	2.5 (0.1)	-91.1 (1.2)	3.5 (0.2)	0.58 (0.1)
p.Val1279Ile	33	103.2 (12.7)	-30.9 (1.7)	2.5 (0.2)	-92.8 (1)	5 (0.6)	0.45 (0.07)
p.Asp1370Gly	35	85.1 (10.6)	-30.6 (1.4)	2.5 (0.2)	-94.7 (1.5)	6.5 (0.9)	*
p.Ala1746Val	26	89.4 (12.7)	-35.4 (2.6)	2.5 (0.1)	-92.2 (1.3)	8.6 (1.2)	*
p.Asp84Asn	16	32.8 (5)	-28.9 (3.1)	3.1 (1.2)	*	*	*
p.Phe93Ser	15	0.2 (0.2)	*	*	*	*	*
p.Asn109Lys	22	119.6 (19.5)	-38.2 (2.6)	2.5 (0.2)	-94.2 (1.5)	5.7 (1)	0.98 (0.1)
p.Leu136Pro	16	39 (6.4)	*	3.3 (0.7)	*	*	*
p.Lys175Asn	15	117.8 (14.5)	-29.5 (3.8)	2.2 (0.2)	-104.6 (2.1)	*	*
p.Ala178Gly	11	109.6 (19.8)	-27.6 (1.6)	2.2 (0.3)	*	*	*
p.Val223Leu	14	34.2 (6.7)	-39.1 (2.9)	2.1 (0.1)	-98.5 (3)	*	*
p.Leu276Gln	14	0.8 (0.6)	*	*	*	*	*
p.Arg282Cys	67	1.3 (0.3)	*	2.6 (0.6)	*	*	*
p.Cys335Arg	24	0 (0)	*	*	*	*	*
p.Glu346Asp	30	113.2 (13.9)	-44.4 (3.2)	1.7 (0.1)	-99.6 (2.4)	13.2 (2)	0.42 (0.07)
p.Asp349Asn	21	28.5 (7.6)	-26.5 (3.1)	*	*	*	*
p.Arg367Cys	25	0.6 (0.4)	*	*	*	*	*
p.Arg367Leu	39	0 (0)	*	*	*	*	*
p.Met369Lys	22	3.4 (0.8)	*	*	*	*	*
p.Gly386Arg	11	1.2 (0.7)	*	*	*	*	*
p.Val396Leu	31	32 (5)	-33.5 (1.4)	2.9 (0.1)	-94.9 (1.3)	5.3 (0.6)	*
p.Met734Val	18	68.1 (8.7)	-36.1 (2.1)	1.6 (0.1)	-103.2 (1.4)	16.2 (1.8)	0.5 (0.11)
p.Ala735Glu	12	0.9 (0.6)	*	*	*	*	*
p.Ala735Thr	25	63.8 (10.1)	-31.4 (1.3)	2.4 (0.2)	-91.6 (0.7)	4.3 (0.4)	0.41 (0.08)
p.Glu746Lys	15	41.7 (10.8)	-36.3 (1.9)	2 (0.1)	-97 (1.4)	7.8 (1.1)	*
p.Met764Lys	30	77.5 (8.6)	-32.9 (2.1)	2.7 (0.2)	-92.5 (1.4)	5.6 (1)	0.27 (0.05)
p.Asp772Asn	41	105.3 (10.8)	-43 (2.5)	1.4 (0.1)	-96.2 (1.5)	8.6 (0.9)	0.51 (0.08)
p.Pro773Ser	41	120.5 (10.5)	-35.1 (1.7)	2.4 (0.1)	-99.3 (1.1)	12.4 (1.6)	0.27 (0.05)
p.Asp785Asn	27	38.9 (7.2)	-25 (1.5)	2.7 (0.3)	-102.6 (1.8)	15.6 (1.4)	0.46 (0.15)
p.Arg808Cys	12	21 (5.1)	-35.8 (1.9)	1.6 (0.1)	-104.1 (1.3)	15.9 (1.4)	*
p.Arg814Gln	36	117.2 (11.7)	-38.9 (1.5)	2.1 (0.1)	-95.7 (1.1)	7.7 (0.8)	1.36 (0.18)
p.Leu839Pro	20	2.9 (2.1)	*	*	*	*	*
p.Phe851Leu	26	16 (2.3)	-32.5 (1.5)	1.8 (0.1)	-95.8 (3.1)	8.8 (3.4)	*

p.Trp879Arg	43	0 (0)	*	*	*	*	*
p.Phe892Ile	23	0.8 (0.6)	*	*	*	*	*
p.Glu901Lys	16	3.2 (0.5)	-32.8 (3)	2.2 (0.4)	*	*	*
p.Asn927Ser	13	29.8 (5.7)	*	*	*	*	*
p.Leu928Pro	27	1.1 (0.8)	*	*	*	*	*
p.Pro1014Ser	34	121.4 (13.2)	-46.6 (1.8)	1.4 (0.1)	-95.9 (1.6)	8.1 (1.1)	0.43 (0.07)
p.Glu1225Lys	19	36 (5.9)	-32.9 (1.3)	2.4 (0.1)	-84 (1.5)	4.2 (0.5)	*
p.Asp1243Asn	42	114.7 (15.2)	-31.1 (1.5)	2.6 (0.1)	-87.7 (1.1)	3.9 (0.9)	0.66 (0.16)
p.Gly1262Ser	10	47 (15.5)	-49 (2.7)	2.3 (0.3)	-97.3 (5.3)	13 (3.2)	*
p.Val1281Phe	39	102.4 (15.5)	-39.6 (1.9)	2.5 (0.1)	-96.8 (1)	8.4 (1.2)	0.81 (0.16)
p.Trp1345Cys	10	12 (2.2)	*	*	*	*	*
p.Leu1346Pro	15	1.6 (0.7)	*	*	*	*	*
p.Val1353Met	31	102.6 (16.5)	-33 (2.3)	2.2 (0.2)	-94 (1.6)	7.4 (0.8)	0.4 (0.11)
p.Asn1380Lys	25	0.2 (0.2)	*	*	*	*	*
p.Ser1382Ile	29	3.5 (0.8)	-40.3 (4)	2.7 (0.6)	*	4.1 (1.1)	*
p.Val1405Leu	15	13.9 (2.8)	-39.4 (2.3)	1.4 (0.1)	-97.1 (3.2)	*	*
p.Val1405Met	14	36 (6)	-26.8 (2.1)	2 (0.3)	*	*	*
p.Gly1406Glu	10	32.6 (6.2)	-42.7 (1.6)	1.9 (0.2)	-98 (2.2)	6.6 (1.2)	*
p.Gly1420Arg	16	3 (1.5)	*	*	*	*	*
p.Gly1420Val	11	0 (0)	*	*	*	*	*
p.Ala1428Val	24	0.3 (0.3)	*	*	*	*	*
p.Tyr1449Cys	12	10.2 (3.4)	*	*	*	*	*
p.Thr1461Ser	41	59.7 (6.3)	-35.7 (1.3)	1.8 (0.1)	-92.5 (1)	4.5 (0.4)	0.63 (0.13)
p.Glu1574Lys	14	43.3 (12.2)	-27 (3.7)	*	*	*	*
p.Arg1583Cys	38	78.9 (7.2)	-39.5 (1.1)	1.8 (0.1)	-96.8 (0.7)	4.7 (0.3)	0.46 (0.06)
p.Gly1642Glu	27	14.8 (2.5)	-33 (1.3)	2.4 (0.2)	-88.9 (2)	3.3 (0.5)	*
p.Gly1661Arg	19	5.4 (1.5)	*	1.6 (0.2)	*	*	*
p.Ser1672Tyr	18	0.9 (0.5)	*	*	*	*	*
p.Ala1680Thr	29	89.5 (14.6)	-42.1 (2.6)	2.2 (0.1)	-96.7 (1.6)	6.8 (1.1)	0.95 (0.2)
p.Thr1709Met	33	23.1 (3.2)	-35.9 (1.3)	2.4 (0.1)	-91.8 (1.2)	3.1 (0.3)	*
p.Asn1722Asp	26	37.2 (3.8)	-29.9 (1.4)	3.3 (0.2)	-89.5 (0.8)	4.2 (0.4)	0.25 (0.13)
p.Pro1730His	31	45.3 (5.1)	-30.1 (1.7)	3.1 (0.2)	-88.2 (1.3)	4.6 (0.6)	0.35 (0.09)
p.Arg1898Cys	13	28.4 (8.6)	-44.4 (3.9)	1.6 (0.1)	-100.7 (1.8)	11.3 (3.5)	*
p.Arg1958Ter	30	59.3 (8.3)	-30.7 (1.7)	2.6 (0.1)	-93.7 (1.4)	4.3 (0.8)	*

This dataset is also available in File S1 in a .csv format. N indicates the total number of cells included for the peak current parameter. The number of analyzed cells for the other parameters are presented in File S1. Only variants with at least 5 qualifying cells were included for non-peak density parameters, so most severe loss of function variants are not included for most parameters.

Table S8. *SCN5A* missense variants with <10% peak current density

Variant	Location	Peak current (% of WT)		PMID	BrS1	LQT3	Unaff.	gnomAD v2.1
		This study	Previous literature					
p.Phe93Ser	N-terminus	0.2	*	*	2	0	0	0
p.Arg104Gln	N-terminus	*	0	23805106	5	0	0	0
p.Arg104Trp	N-terminus	*	0	22739120	2	0	0	1
p.Arg121Trp	N-terminus	0.7	0	20395683	3	0	0	0
p.Thr187Ile	DI S2-S3 linker	*	0	16325048	1	0	0	0
p.Leu276Gln	DI S5-P linker	0.8	*	*	2	0	0	0
p.Arg282Cys	DI S5-P linker	1.3	*	*	2	0	1	0
p.Arg282His	DI S5-P linker	*	5	21840964	4	0	0	4
p.Cys335Arg	DI S5-P linker	0	*	*	2	0	0	0
p.Thr353Ile	DI S5-P linker	0.1	8.3	17198989	5	0	0	0
p.Asp356Asn	DI S5-P linker	*	0	16325048	9	0	0	1
p.Arg367Cys	DI S5-P linker	0.6	*	*	3	2	0	3
p.Arg367Leu	DI S5-P linker	0	*	*	1	0	0	0
p.Met369Lys	DI S5-P linker	3.4	*	*	3	0	0	0
p.Gly386Arg	DI S6	1.2	*	*	2	0	0	0
p.Ala735Glu	DII S1	0.9	*	*	2	0	0	0
p.Gly752Arg	DII S2	23.2	6.3	12693506	8	0	1	1
p.Leu839Pro	DII S5	2.9	*	*	4	0	1	0
p.Leu846Arg	DII S5	*	0	22028457	1	0	0	0
p.Arg878Cys	DII S5-P linker	*	0	18616619	32	0	4	0
p.Arg878His	DII S5-P linker	*	0	25904541	5	0	0	0
p.Trp879Arg	DII S5-P linker	0	*	*	2	0	0	0
p.Phe892Ile	DII S5-P linker	0.8	*	*	2	0	0	0
p.Arg893His	DII S5-P linker	*	0	25904541	6	0	3	1
p.Gly897Glu	DII S5-P linker	*	0	25904541	0	1	0	0
p.Glu901Lys	DII S5-P linker	3.2	*	*	6	0	0	0
p.Ser910Leu	DII S6	*	0	24768612	4	0	0	1
p.Leu928Pro	DII S6	1.1	*	*	1	0	0	0
p.Ser1218Ile	DIII S1	*	0	23424222	3	0	0	0
p.Leu1346Pro	DIII S5	1.6	*	*	2	0	0	0
p.Asn1380Lys	DIII S5-P linker	0.2	*	*	2	0	0	0
p.Ser1382Ile	DIII S5-P linker	3.5	*	*	3	0	5	0
p.Gly1406Arg	DIII S5-P linker	*	7.7	16632547	4	0	1	0
p.Gly1408Arg	DIII S5-P linker	*	0	14523039	8	1	19	0
p.Gly1420Arg	DIII S5-P linker	3	*	*	3	0	0	0
p.Gly1420Val	DIII S5-P linker	0	*	*	2	0	0	0
p.Ala1428Val	DIII S5-P linker	0.3	*	*	4	0	2	0
p.Asp1430Asn	DIII S5-P linker	*	0	23612926	2	0	0	0
p.Arg1432Gly	DIII S5-P linker	2.2	0	10727653	1	0	0	0
p.Ile1660Val	DIV S5	*	1.5	17075016	5	2	2	0
p.Gly1661Arg	DIV S5	5.4	*	*	7	0	0	0
p.Ser1672Tyr	DIV S5	0.9	*	*	3	0	0	0
p.Gly1712Cys	DIV Pore Helix	*	0	28219873	1	0	0	0
p.Gly1740Arg	DIV P-S6 Loop	*	0	15057319	2	0	0	0
p.Gly1743Glu	DIV P-S6 Loop	*	0	16945804	10	0	0	0
p.Gly1743Arg	DIV P-S6 Loop	*	0	15023552	12	0	6	0

File S1. Summary of patch clamp data for each variant (.csv)

For each variant, peak current density (normalized to wild-type), voltage of ½ activation, inactivation time, voltage of ½ inactivation, recovery from inactivation, and late current (% of peak) are presented. Means, standard errors of the mean, and the number of qualifying cells are presented for each parameter. Some parameters have "normalized" values also included which indicates the difference in the parameter value from wild-type. Only variants with at least 5 qualifying cells are included, so most severe loss of function variants are not included for most parameters. In addition, variants are classified into categories based on their functional properties, and each variant's BS3 and PS3 ACMG criteria for Brugada Syndrome (loss of function) or Long QT syndrome (gain of function) is presented.

Supplemental Methods

Peak current averaging

For each variant, mean peak current density was calculated as *peak current/capacitance*, averaged across all in voltage control cells. For variants with near-wild-type peak currents, the percentage of cells with detectable currents matched the expected percentage from flow cytometry (Figure 1A-B). However, severe loss of function variants had a substantially lower proportion of wells with detectable currents compared to the predicted percentage from flow cytometry, as is typically observed.[6] Since a simple mean would overestimate the true peak current, an adjustment was made to the means based on a comparison between the flow cytometry and patch clamp data. If the percentage of current-positive wells was >10% less than the expected percentage from flow cytometry, the number of expected additional cells with no current was calculated as follows:

*Expected additional cells = #QC+ cells *(%mCherry+ cells - %QC+ cells with current)*

QC+ cells are defined as cells with a 0.5- 10 GΩ seal resistance and 5-30 pF capacitance. These expected additional cells were added to the peak current density average. For each variant, peak current density averages were first normalized to wild-type cells from the same experiment/transfection, then averaged across independent experiments/transfections.

Building a homology model

Two starting partial models of SCN5A bound with SCN1B, which only covered aligned residues, were generated by threading the sequences of SCN5A and SCN1B onto the two template structures respectively. The threading was guided by the corresponding sequence alignments. Full models were created by hybridization of the two starting models using the

Rosetta comparative modeling (RosettaCM) protocol[7] guided by the RosettaMembrane energy function.[8] The starting model generated from the primary template was used as the base model during hybridization. The boundaries of membrane-spanning segments were calculated using the PPM server[9] based on the starting model generated from the primary template. The boundaries were used to impose membrane-specific Rosetta energy terms on residues within the theoretical membrane bilayer. Fragments in the starting model where coordinates were missing were modeled *de novo* by inserting fragments selected from the Protein Data Bank using local sequence information.[10] Amino acid rotamer conformations were optimized by a nondeterministic Monte Carlo simulated annealing protocol, referred to as rotamer repacking in Rosetta, and models were refined in internal and Cartesian coordinate space by gradient-based minimization. A total of 6000 full models of SCN5A bound with SCN1B were generated using RosettaCM and models ranked by Rosetta energy function in the top 20% were grouped into ten clusters based on pairwise root-mean-square distances. The lowest-energy model from the largest cluster was selected as the final model (Figure 5, S5) for structure-based analysis in this work. This model was also the lowest-energy model across all models sampled.

ΔΔG Calculations

The Rosetta ΔΔG protocol samples conformational degrees of freedom in a locally restricted region around the residue of interest: all sidechains within 6 Å of the mutated residue, and the backbone of a three-residue window around the mutated residue were allowed to move.[11] The sampling was guided by an energy function fitted to recapitulate experimentally determined membrane protein ΔΔG values (Table S6).[12] ΔΔG values computed through this energy function were previously demonstrated to be strongly correlated with cell surface expression levels of human rhodopsin variants.[13] Previous studies have shown that the

magnitude of variant-caused perturbation to protein native thermostability (i.e. $|\Delta\Delta G|$) correlates best with disease likelihood.[14] Accordingly, in this work, variant-induced perturbation to native thermostability ($|\Delta\Delta G_{wild\text{-}type\text{->}variant}|$) was computed as the absolute energy difference between the refined variant structure and the refined wild-type structure: $|\Delta\Delta G_{wild\text{-}type\text{->}variant}| = |\Delta G_{variant} - \Delta G_{wild\text{-}type}|$. Due to the nondeterministic nature of conformation sampling in Rosetta, the $|\Delta\Delta G|$ of each variant was computed 30 times and the average was recorded. The Rosetta energy function is a hybrid of both physically meaningful terms and statistics-based terms, and it does not compute the entropic contribution to the Gibbs free energy in a thermodynamically rigorous manner.[15] Thus, it is best to interpret $\Delta\Delta G$ values computed through the Rosetta energy function in a statistical manner as approximations to the Gibbs free energies.

Literature Cited

1. Richards, S., Aziz, N., Bale, S., Bick, D., Das, S., Gastier-Foster, J., Grody, W.W., Hegde, M., Lyon, E., Spector, E., et al. (2015). Standards and guidelines for the interpretation of sequence variants: a joint consensus recommendation of the American College of Medical Genetics and Genomics and the Association for Molecular Pathology. Genet Med 17, 405-424.
2. Potet, F., Mabo, P., Le Coq, G., Probst, V., Schott, J.J., Airaud, F., Guihard, G., Daubert, J.C., Escande, D., and Le Marec, H. (2003). Novel brugada SCN5A mutation leading to ST segment elevation in the inferior or the right precordial leads. J Cardiovasc Electrophysiol 14, 200-203.
3. Benson, D.W., Wang, D.W., Dyment, M., Knilans, T.K., Fish, F.A., Strieper, M.J., Rhodes, T.H., and George, A.L., Jr. (2003). Congenital sick sinus syndrome caused by recessive mutations in the cardiac sodium channel gene (SCN5A). J Clin Invest 112, 1019-1028.
4. Kroncke, B.M., Glazer, A.M., Smith, D.K., Blume, J.D., and Roden, D.M. (2018). SCN5A (NaV1.5) Variant Functional Perturbation and Clinical Presentation: Variants of a Certain Significance. Circ Genom Precis Med 11, e002095.
5. Kroncke, B.M.S., D.; Glazer, A.; Roden, D.; Blume, J. (2019). A Bayesian method using sparse data to estimate penetrance of disease-associated genetic variants. bioRxiv: https://wwwbiorxivorg/content/101101/571158v1.
6. Pfahnl, A.E., Viswanathan, P.C., Weiss, R., Shang, L.L., Sanyal, S., Shusterman, V., Kornblit, C., London, B., and Dudley, S.C., Jr. (2007). A sodium channel pore mutation causing Brugada syndrome. Heart Rhythm 4, 46-53.
7. Song, Y., DiMaio, F., Wang, R.Y., Kim, D., Miles, C., Brunette, T., Thompson, J., and Baker, D. (2013). High-resolution comparative modeling with RosettaCM. Structure 21, 1735-1742.
8. Barth, P., Wallner, B., and Baker, D. (2009). Prediction of membrane protein structures with complex topologies using limited constraints. Proc Natl Acad Sci U S A 106, 1409-1414.
9. Lomize, M.A., Pogozheva, I.D., Joo, H., Mosberg, H.I., and Lomize, A.L. (2012). OPM database and PPM web server: resources for positioning of proteins in membranes. Nucleic Acids Research 40, D370-D376.
10. Simons, K.T., Kooperberg, C., Huang, E., and Baker, D. (1997). Assembly of protein tertiary structures from fragments with similar local sequences using simulated annealing and Bayesian scoring functions. J Mol Biol 268, 209-225.
11. Park, H., Bradley, P., Greisen, P., Liu, Y., Mulligan, V.K., Kim, D.E., Baker, D., and DiMaio, F. (2016). Simultaneous Optimization of Biomolecular Energy Functions on Features from Small Molecules and Macromolecules. Journal of Chemical Theory and Computation 12, 6201-6212.
12. Kroncke, B.M., Duran, A.M., Mendenhall, J.L., Meiler, J., Blume, J.D., and Sanders, C.R. (2016). Documentation of an Imperative To Improve Methods for Predicting Membrane Protein Stability. Biochemistry 55, 5002-5009.
13. Roushar, F.J., Gruenhagen, T.C., Penn, W.D., Li, B., Meiler, J., Jastrzebska, B., and Schlebach, J.P. (2019). Contribution of Cotranslational Folding Defects to Membrane Protein Homeostasis. J Am Chem Soc 141, 204-215.

14. Casadio, R., Vassura, M., Tiwari, S., Fariselli, P., and Luigi Martelli, P. (2011). Correlating disease-related mutations to their effect on protein stability: a large-scale analysis of the human proteome. Hum Mutat 32, 1161-1170.
15. Alford, R.F., Leaver-Fay, A., Jeliazkov, J.R., O'Meara, M.J., DiMaio, F.P., Park, H., Shapovalov, M.V., Renfrew, P.D., Mulligan, V.K., Kappel, K., et al. (2017). The Rosetta All-Atom Energy Function for Macromolecular Modeling and Design. J Chem Theory Comput 13, 3031-3048.